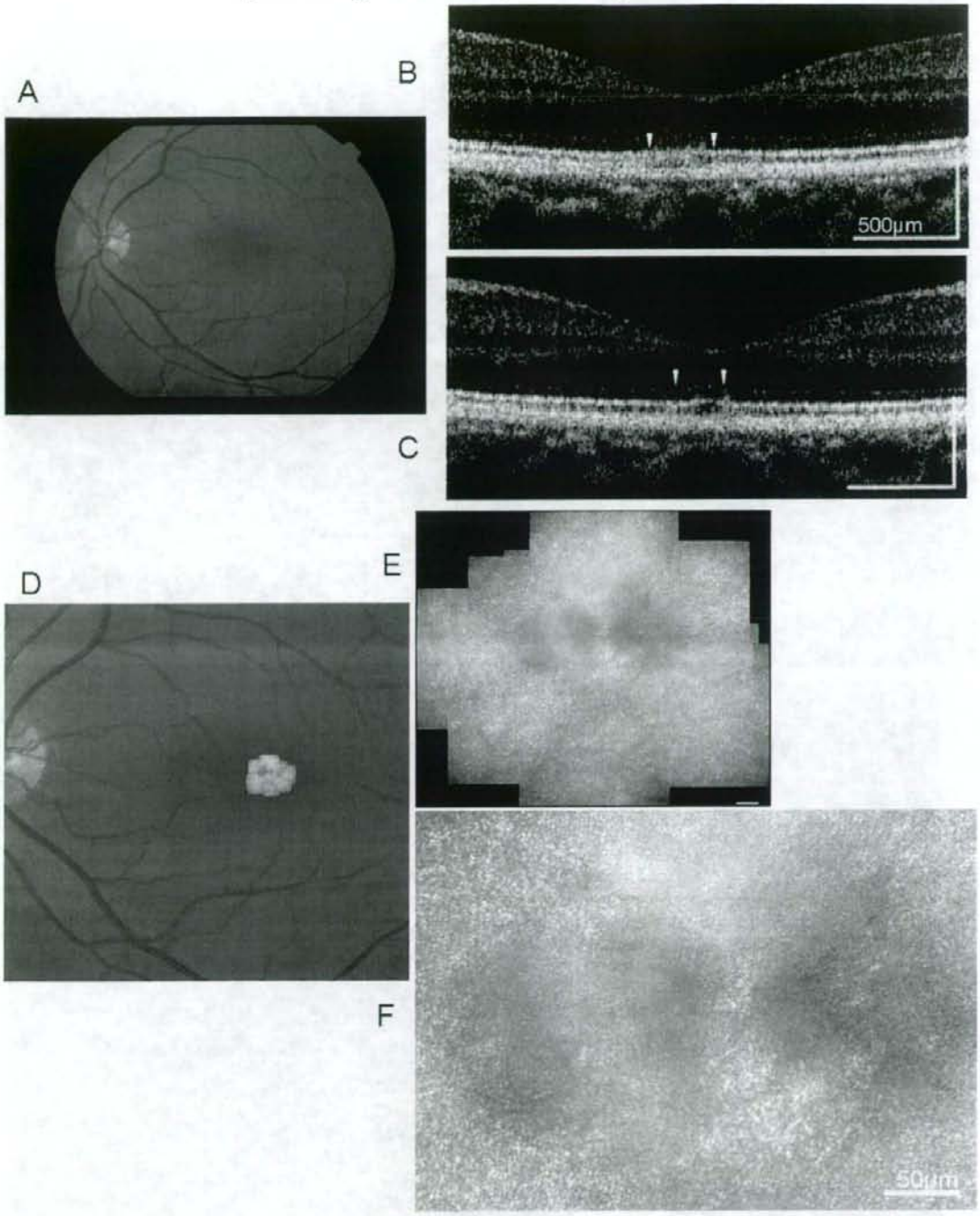

Figure 1. Images from the left eye of patient 1, who sought treatment for metamorphopsia. **A**, Fundus photograph showing normal appearance. **B**, Fourier-domain optical coherence tomography image (5-mm horizontal scan) demonstrating the disturbance of the inner segment/outer segment (IS/OS) junction and outer segment (OS) layer (between the second and third lines) for approximately 330 μm. **C**, Fourier-domain optical coherence tomography vertical scan showing the disturbance of the IS/OS junction and OS layer for approximately 150 μm. The arrowhead in **B** and **C** point to the area of IS/OS and OS disturbances. The horizontal bars in **B** and **C** represent 500 μm. **D**, Montage of adaptive optics (AO) image superimposed on the fundus photograph. **E**, Montage of adaptive optics image (low magnification). **F**, Magnified AO image of the fovea showing a dark area (disappearance of cone mosaic) at the fovea just above the fixation point. The shape of dark area was geographic and the size was approximately 350 μm horizontally and 180 μm vertically. The horizontal bars in **E** and **F** represent 50 μm.

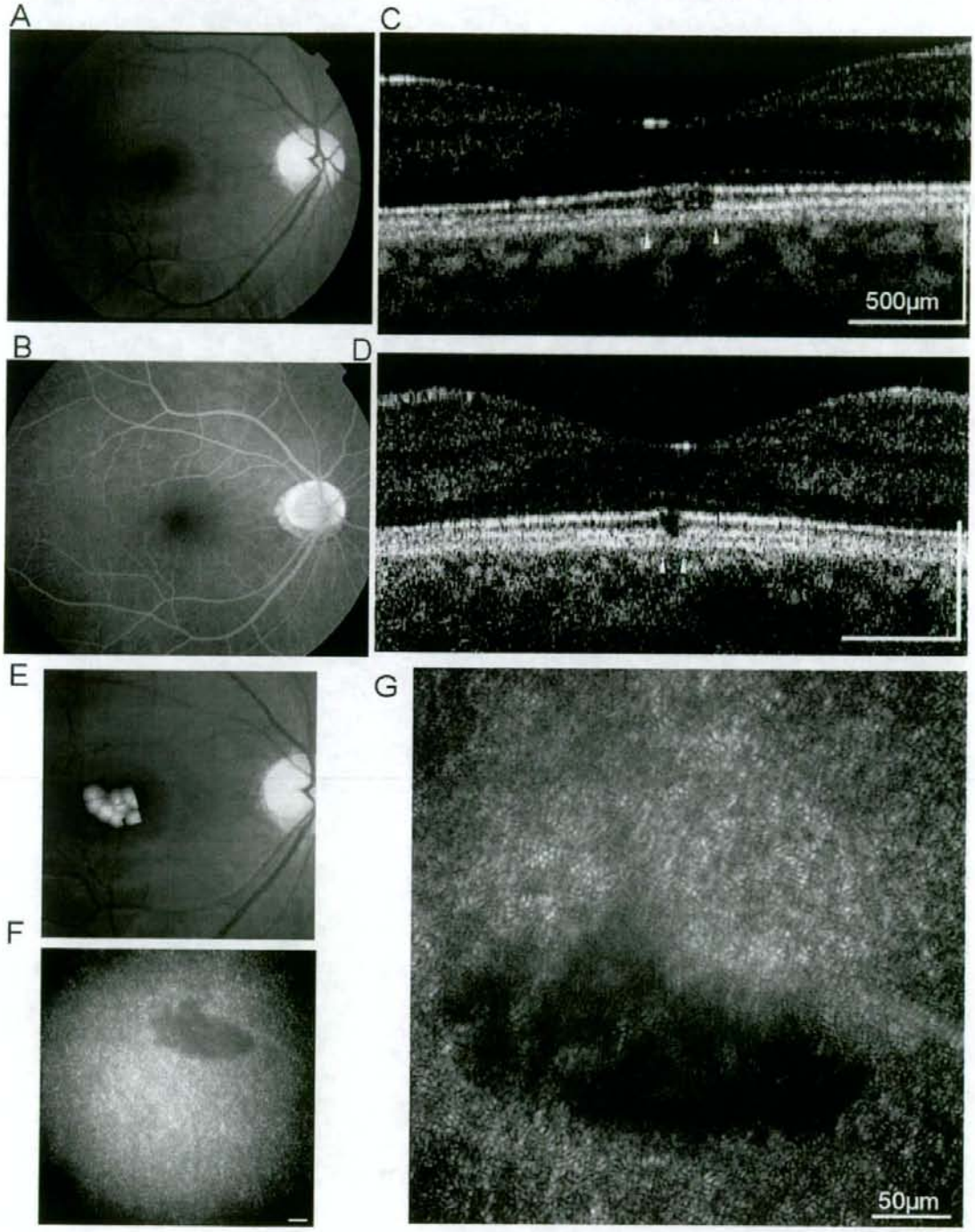

Figure 2. Images from the right eye of patient 2, who sought treatment for metamorphopsia. **A**, Fundus photograph showing that the retina appears to be normal. **B**, Early-phase fluorescein angiography image showing normal results. **C** and **D**, Fourier-domain optical coherence tomography images demonstrating a defect of outer segment (OS) layer in the fovea that was located just beneath the inner segment/OS junction. The size of the defect was (**C**) 280 μm on the horizontal scan and (**D**) 100 μm on the vertical scan. The IS/OS line was preserved but the intensity was slightly low. The arrowhead in **C** and **D** points to the area of OS defect. The horizontal bars in **C** and **D** represent 500 μm, and the vertical bars represent 200 μm. **E**, Montage of adaptive optics (AO) image superimposed on the fundus photograph. **F**, adaptive optics image (low magnification). **G**, Magnified AO image of the fovea showing a dark oval-shaped area (disappearance of cone mosaic) with a size of 300 μm horizontally and 120 μm vertically. The horizontal bars in **F** and **G** represent 50 μm.

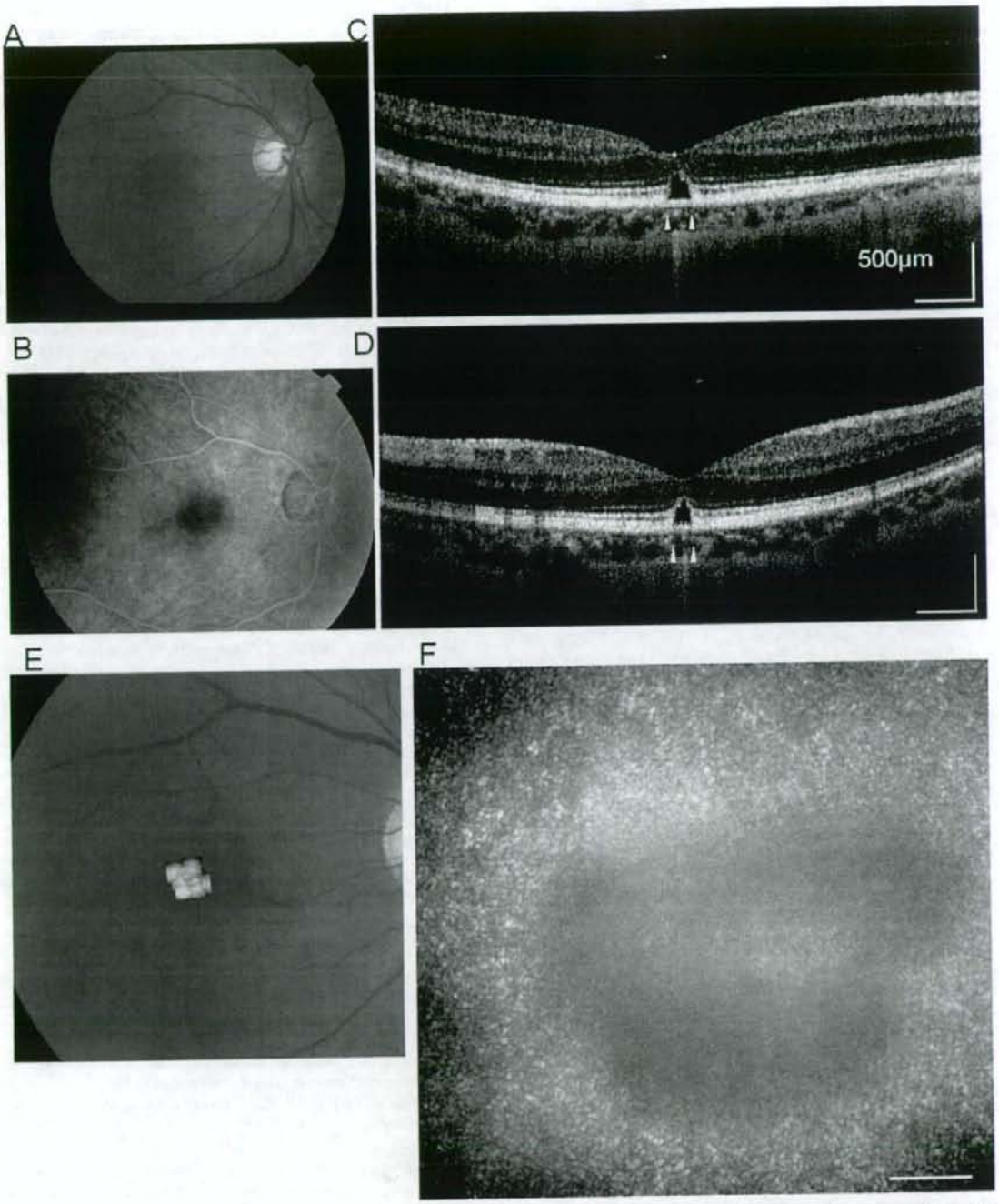

Figure 3. Images from the right eye of patient 3, who sought treatment for metamorphopsia. **A**, Fundus photograph showing normal appearance. **B**, Early-phase of fluorescein angiography image showing normal results. **C** and **D**, Fourier-domain optical coherence tomography images demonstrating the elevation of the external limiting membrane. Photoreceptor outer segment (OS) and inner segment/OS junction are not present in an area of (**C**) 200 μm on the horizontal scan and (**D**) 150 μm on the vertical scan. The arrowhead in **C** and **D** indicates the area of OS defect. The horizontal bars in **C** and **D** represent 500 μm, and the vertical bars represent 200 μm. **E**, Montage of adaptive optics (AO) image superimposed on the fundus photograph. **F**, Magnified image of AO image in the fovea demonstrating a dark oval-shaped area (disappearance of cone mosaic) with a size of 300 μm horizontally and 200 μm vertically. At the fovea centralis, a slightly high reflective area without cone mosaic was observed. The horizontal bars in **F** represent 50 μm.

References

1. Brockhurst RJ, Sandberg MA. Optical coherence tomography findings in occult macular dystrophy. Am J Ophthalmol 2007; 143:516–8.
2. Kondo M, Ito Y, Ueno S, et al. Foveal thickness in occult macular dystrophy. Am J Ophthalmol 2003;135:725–8.
3. Benhamou N, Souied EH, Zolf R, et al. Adult-onset foveomacular vitelliform dystrophy: a study by optical coherence tomography. Am J Ophthalmol 2003;135:362–7.
4. Sandberg MA, Brockhurst RJ, Gaudio AR, Berson EL. The association between visual acuity and central retinal thickness in retinitis pigmentosa. Invest Ophthalmol Vis Sci 2005;46: 3349–54.
5. Samsel A, Drobecka-Brydak E, Godowska-Brydak E, et al. Optical coherence tomography in Stargardt's dystrophy [in Polish]. Klin Oczna 2005;107:668–71.
6. Miyake Y, Horiguchi M, Tomita N, et al. Occult macular dystrophy. Am J Ophthalmol 1996;122:644–53.
7. Ergun E, Hermann B, Wirtitsch M, et al. Assessment of central visual function in Stargardt's disease/fundus flavimaculatus with ultrahigh-resolution optical coherence tomography. Invest Ophthalmol Vis Sci 2005;46:310–6.
8. Wirtitsch E, Ergun B, Hermann A, et al. Ultrahigh resolution optical coherence tomography in macular dystrophy. Am J Ophthalmol 2005;140:976–83.
9. Drexler W, Sattmann H, Hermann B, et al. Enhanced visualization of macular pathology with the use of ultrahigh-resolution optical coherence tomography. Arch Ophthalmol 2003;121:695–706.
10. Ojima Y, Hangai M, Sasahara M, et al. Three-dimensional imaging of the foveal photoreceptor layer in central serous chorioretinopathy using high-speed optical coherence tomography. Ophthalmology 2007;114:2197–207.
11. Schocket LS, Witkin AJ, Fujimoro JG, et al. Ultrahigh-resolution optical coherence tomography in patients with decreased visual acuity after retinal detachment repair. Ophthalmology 2006;113:666–72.
12. Alam S, Zawadski RJ, Choi S, et al. Clinical application of rapid serial Fourier-domain optical coherence tomography for macular imaging. Ophthalmology 2006;113:1425–31.
13. Piccolino FC, de la Longrais RR, Ravera G, et al. The foveal photoreceptor layer and visual acuity loss in central serous chorioretinopathy. Am J Ophthalmol 2005;139:87–99.
14. Iida T, Hagimura N, Sato T, Kishi S. Evaluation of central serous chorioretinopathy with optical coherence tomography. Am J Ophthalmol 2000;129:16–20.
15. Pircher M, Baumann B, Gotzinger E, Hitzenberger CK. Retinal cone mosaic imaged with transverse scanning optical coherence tomography. Optics Lett 2006;15:1821–3.
16. Liang J, Williams DR, Miller DT. Supernormal vision and high-resolution retinal imaging through adaptive optics. J Opt Soc Am A Opt Image Sci Vis 1997;14:2884–92.
17. Roorda A, Williams DR. The arrangement of the three cone classes in the living human eye. Nature 1999;397:520–2.
18. Roorda A, Williams DR. Optical fiber properties of individual human cones. J Vis 2002;2:404–12.
19. Roorda A, Romero-Borja F, Donnelly W III, et al. Adaptive optics scanning laser ophthalmoscopy. Opt Express [serial online] 2002;10:405–12. Available at: http://www.opticsexpress.org/abstract.cfm?id=68843. Accessed March 11, 2008.
20. Pallikaris A, Williams DR, Hofer H. The reflectance of single cones in the living human eye. Invest Ophthalmol Vis Sci 2003;44:4580–92.
21. Wolfing JI, Chung M, Carroll J, et al. High-resolution retinal imaging of cone-rod dystrophy. Ophthalmology 2006;113: 1014–9.
22. Choi SS, Double N, Hardy JL, et al. In vivo imaging of the photoreceptor mosaic in retinal dystrophies and correlations with visual function. Invest Ophthalmol Vis Sci 2006;47: 2080–92.
23. Duncan JL, Zhang Y, Gandhi J, et al. High-resolution imaging with adaptive optics in patients with inherited retinal degeneration. Invest Ophthalmol Vis Sci 2007;48:3283–91.
24. Kitaguchi Y, Bessho K, Yamaguchi T, et al. In vivo measurements of cone photoreceptor spacing in myopic eyes from images obtained by an adaptive optics fundus camera. Jpn J Ophthalmol 2007;51:456–61.
25. Zawadzki RJ, Choi SS, Jones SM, et al. Adaptive optics-optical coherence tomography: optimizing visualization of microscopic retinal structures in three dimensions. J Opt Soc Am A Opt Image Sci Vis 2007;24:1373–83.
26. Douglas RS, Duncan J, Brucker A, et al. Foveal spot: a report of thirteen patients. Retina 2003;23:348–53.
27. Zambarakji HJ, Schlottmann P, Tanner V, et al. Macular microholes: pathogenesis and natural history. Br J Ophthalmol 2005;89:189–93.

Footnotes and Financial Disclosures

Originally received: November 25, 2007.
Final revision: March 16, 2008.
Accepted: March 25, 2008.
Available online: May 16, 2008. Manuscript no. 2007-1518.

[1] Department of Applied Visual Science, Osaka University Graduate School of Medicine, Osaka, Japan.

[2] Department of Ophthalmology, Osaka University Graduate School of Medicine, Osaka, Japan.

[3] Topcon Research Institute, Tokyo, Japan.

Financial Disclosure(s):
The funding organization had no role in the design or conduct of this research.

Supported by the Ministry of Health, Labor and Welfare, Tokyo, Japan (Health Sciences Research grant no.: H19-sensory-001).

Tatsuo Yamaguchi, Naoki Nakazawa, and Toshifumi Mihashi are employees of Topcon.

Correspondence:
Takashi Fujikado, MD, Department of Applied Visual Science, Osaka University Graduate School of Medicine, 2-2 Yamadaoka, Suita, Osaka 565-0871, Japan. E-mail: fujikado@ophthal.med.osaka-u.ac.jp.

Potent Inhibition of Cicatricial Contraction in Proliferative Vitreoretinal Diseases by Statins

Shuhei Kawahara,[1] Yasuaki Hata,[1] Takeshi Kita,[1] Ryoichi Arita,[1] Muneki Miura,[1] Shintaro Nakao,[2] Yasutaka Mochizuki,[1] Hiroshi Enaida,[1] Tadahisa Kagimoto,[3] Yoshinobu Goto,[4] Ali Hafezi-Moghadam,[2] and Tatsuro Ishibashi[1]

OBJECTIVE—Despite tremendous progress in vitreoretinal surgery, certain postsurgical complications limit the success in the treatment of proliferative vitreoretinal diseases (PVDs), such as proliferative diabetic retinopathy (PDR) and proliferative vitreoretinopathy (PVR). One of the most significant complications is the cicatricial contraction of proliferative membranes, resulting in tractional retinal detachment and severe vision loss. Novel pharmaceutical approaches are thus urgently needed for the management of these vision-threatening diseases. In the current study, we investigated the inhibitory effects of statins on the progression of PVDs.

RESEARCH DESIGN AND METHODS—Human vitreous concentrations of transforming growth factor-β2 (TGF-β2) were measured by enzyme-linked immunosorbent assay. TGF-β2– and vitreous-dependent phosphorylation of myosin light chain (MLC), a downstream mediator of Rho-kinase pathway, and collagen gel contraction simulating cicatrical contraction were analyzed using cultured hyalocytes. Inhibitory effects of simvastatin on cicatrical contraction were assessed both in vitro and in vivo.

RESULTS—Human vitreous concentrations of TGF-β2 were significantly higher in the samples from patients with PVD compared with those without PVD. Simvastatin inhibited TGF-β2–dependent MLC phosphorylation and gel contraction in a dose- and time-dependent manner and was capable of inhibiting translocation of Rho protein to the plasma membrane in the presence of TGF-β2. Vitreous samples from patients with PVD enhanced MLC phosphorylation and gel contraction, whereas simvastatin almost completely inhibited these phenomena. Finally, intravitreal injection of simvastatin dose-dependently prevented the progression of diseased states in an in vivo model of PVR.

CONCLUSIONS—Statins might have therapeutic potential in the prevention of PVDs. ***Diabetes*** **57:2784–2793, 2008**

From the [1]Department of Ophthalmology, Graduate School of Medical Sciences, Kyushu University, Maidashi, Higashi-Ku, Fukuoka, Japan; the [2]Massachusetts Eye and Ear Infirmary, Department of Ophthalmology, Harvard Medical School, Boston, Massachusetts; [3]Aqumen Biopharmaceuticals, Tenjin, Chuo-Ku, Fukuoka, Japan; and the [4]Department of Occupational Therapy, Faculty of Rehabilitation, International University of Health and Welfare at Okawa, Enokizu, Okawa, Fukuoka, Japan.

Corresponding author: Yasuaki Hata, hatachan@med.kyushu-u.ac.jp.

Received 2 March 2007 and accepted 26 June 2008.

Published ahead of print at http://diabetes.diabetesjournals.org on 3 July 2008. DOI: 10.2337/db08-0302.

Proliferative vitreoretinal diseases (PVDs), such as proliferative diabetic retinopathy (PDR) and proliferative vitreoretinopathy (PVR), are common causes of severe vision loss (1). Surgical approaches for the treatment of these diseases have evolved significantly in the recent past, but the occurrence of postoperative complications, such as cicatricial contraction, limit the therapeutic success (2). Therefore, there is an urgent need for alternate pharmacological treatments of PVDs that can complement or potentially replace surgical intervention. In PDR and PVR, excessive wound healing and fibrosis induce the formation of proliferative membranes on the retinal surface. The proliferative membrane then extends into the vitreous and contracts, causing tractional detachment (3). The proliferative membrane consists of various cells, including hyalocytes, retinal pigment epithelial cells, glial cells, and fibroblast-like cells (4–7).

Hyalocytes morphologically resemble macrophages and are considered to originate from peripheral blood monocytes (8). Under physiological conditions, hyalocytes are mainly located in the cortical vitreous and are considered to maintain its transparency (9,10). Under pathological conditions, hyalocytes are thought to be critical in vitreoretinal interface diseases, such as idiopathic epiretinal membrane formation, macular hole, and diabetic macular edema (11). Hyalocytes in diabetic eyes are higher in number and of different shape compared with those in normal eyes (12).

Transforming growth factor-β (TGF-β) is pivotal to tissue fibrosis. Among the three isoforms of TGF-β, TGF-β2 is the predominant isoform in the vitreous (13,14). We and others have shown that TGF-β2 is overexpressed in the epiretinal membrane and vitreous of PDR and PVR patients and that its expression correlates with the presence of intraocular fibrosis (14–17). TGF-β2 modulates the differentiation of various cell types and is considered to increase the production of extracellular matrix, resulting in the formation and contraction of proliferative membranes (18,19). Thus, it is possible that the combination of hyalocytes and TGF-β2 may contribute to the pathogenesis of PVDs.

Statins, inhibitors of the 3-hydroxy-3-methyl-glutaryl (HMG)-CoA reductase, are widely used to reduce endogenous cholesterol synthesis and improve hypercholesterolemia (20). HMG-CoA reductase is an upstream enzyme in the mevalonate biosynthetic pathway that catalyzes the conversion of HMG-CoA into mevalonate and then, in a number of steps, into farnesylpyrophosphate (FPP), a precursor of cholesterol (21). By inhibiting HMG-CoA reductase, statins block the mevalonate pathway, resulting

in reduced synthesis of FFP and cholesterol. Statins are divided into three categories: the natural (i.e., lovastatin and pravastatin), the semisynthetic (i.e., simvastatin), and the synthetic (i.e., atorvastatin, fluvastatin, and cerivastatin). Statins decrease the risk for cardiovascular events even among high-risk individuals with coronary disease and diabetes (22). Moreover, statins may be useful in the treatment of other conditions, such as osteoporosis (23) and cancer growth and metastasis (24,25).

Another product of the mevalonate pathway is geranylgeranylpyrophosphate (GGPP), which is synthesized from FPP. Both FPP and GGPP are important isoprenoid intermediates and serve as lipid attachments for a variety of intracellular proteins to the plasma membrane, including the γ-subunit of heterotrimeric G-proteins and the small GTP-binding proteins, such as Ras and Rho, resulting in their activation (26). Rho translocation from the cytoplasm to the plasma membrane is dependent on geranylgeranylation (GGPP attachment), whereas Ras translocation is dependent on farnesylation (FPP attachment) (27). Rho in the plasma membrane is implicated in the cytoskeletal responses to extracellular signals and is converted to an active GDP-bound state (28). Rho-kinase, one of the effector molecules of Rho, is involved in a variety of cellular events related to cell morphology, adhesion, and motility (28–30), especially through phosphorylation of the myosin light chain (MLC). MLC phosphorylation induces actin-myosin interaction and, consequently, smooth muscle contraction and stress fiber formation in nonmuscle cells (31,32). Activation of the Rho/Rho-kinase pathway is therefore indispensable for smooth muscle contraction. GGPP is one of the downstream components of the mevalonate pathway and plays an important part in the Rho/Rho-kinase pathway activation. Thus, statins, which regulate the mevalonate pathway, also regulate the Rho/Rho-kinase pathway and, consequently, MLC phosphorylation.

Previously, we reported that the Rho-kinase pathway is involved in TGF-β2–induced MLC phosphorylation and contraction of hyalocyte-containing collagen gels and that hydroxyfasudil, a potent Rho-kinase inhibitor, significantly diminishes these TGF-β2–induced effects (18). In the present study, we investigate the regulatory effects of statins on TGF-β2– and vitreous-dependent MLC phosphorylation and contraction of hyalocyte-containing collagen gels and their therapeutic potential for prevention of PVDs in vivo.

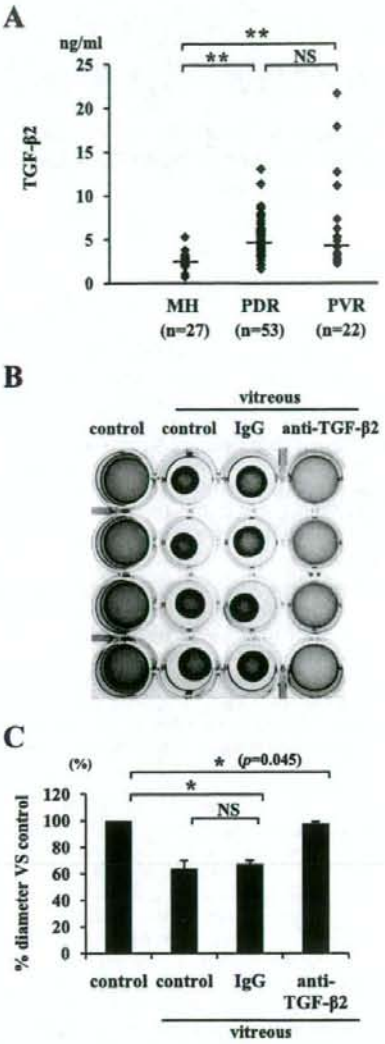

FIG. 1. TGF-β2 expression in the vitreous. *A*: Vitreous samples were collected from patients with non-PVD (macular hole) and PVD (PDR and PVR). Concentrations of TGF-β2 in the vitreous were measured by enzyme-linked immunosorbent assay (macular hole, $n = 27$; PDR, $n = 53$; PVR, $n = 22$). $^{**}P < 0.01$ compared with macular hole. *B*: Hyalocytes were embedded in type I collagen gels ($n = 4$). After starvation and pretreatment with 1 μg/ml anti–TGF-β2 antibody or 1 μg/ml IgG for 1 h, the collagen gels were treated with vitreous samples from patients with PVD. Five days after the treatment, the gels were photographed. *C*: The diameter of the collagen gels was measured and expressed as percentage of the average diameter of the control group. $^{*}P < 0.05$.

RESEARCH DESIGN AND METHODS

Reagents. Simvastatin, fluvastatin, pravastatin, and cerivastatin were purchased from CalBiochem (La Jolla, CA). Lovastatin was purchased from Funakoshi (Tokyo). Simvastatin was used as an active form after treatment with NaOH.

Vitreous samples and enzyme-linked immunosorbent assay. This study was carried out with approval from the Institutional Review Board and performed in accordance with the ethical standards of the 1989 Declaration of Helsinki. We obtained written informed consent from the patients. Vitreous samples were collected from patients who underwent pars plana vitrectomy because of non-PVD (macular hole) or PVD (PDR and PVR). Concentrations of TGF-β2 were measured by a human TGF-β2 immunoassay kit (R&D Systems, Minneapolis, MN).

Cell culture. Bovine hyalocytes were isolated as we previously reported (33). Cultured hyalocytes obtained between passages 5 and 7 were used in experiments.

Collagen gel contraction assay. The contraction assay was performed as we previously described (33). Type I collagen (Koken, Tokyo), a reconstitution buffer, hyalocytes suspension, and distilled water were mixed and added to a 24-multiwell plate (Nunc, Roskilde, Denmark). After 1-h pretreatment of vitreous samples with 1 μg/ml anti–TGF-β2 antibody (R&D Systems) or 1 μg/ml mouse IgG (Sigma-Aldrich) that was added for confirming the absence of nonspecific suppression of the gel contraction by anti–TGF-β2 antibody, the gels were treated with the vitreous samples (400 μl). The diameter of the collagen gel was measured at 5 days after the treatment. For quantitative purposes, contraction data are presented as the reduction in diameter of the collagen gels.

In the same way, collagen gels containing hyalocytes were starved, pretreated with statins for 24 h, and then treated with 3 ng/ml TGF-β2 (Sigma-Aldrich) or vitreous samples.

Western blot analysis. Total cell lysates were subjected to 15% SDS-PAGE, and the blots were incubated with an antibody against phosphorylated-MLC (*p*-MLC; 1:1,000; Santa Cruz Biotechnology, Santa Cruz, CA). Visualization was performed with an enhanced chemiluminesence (ECL; Amersham, Arlington

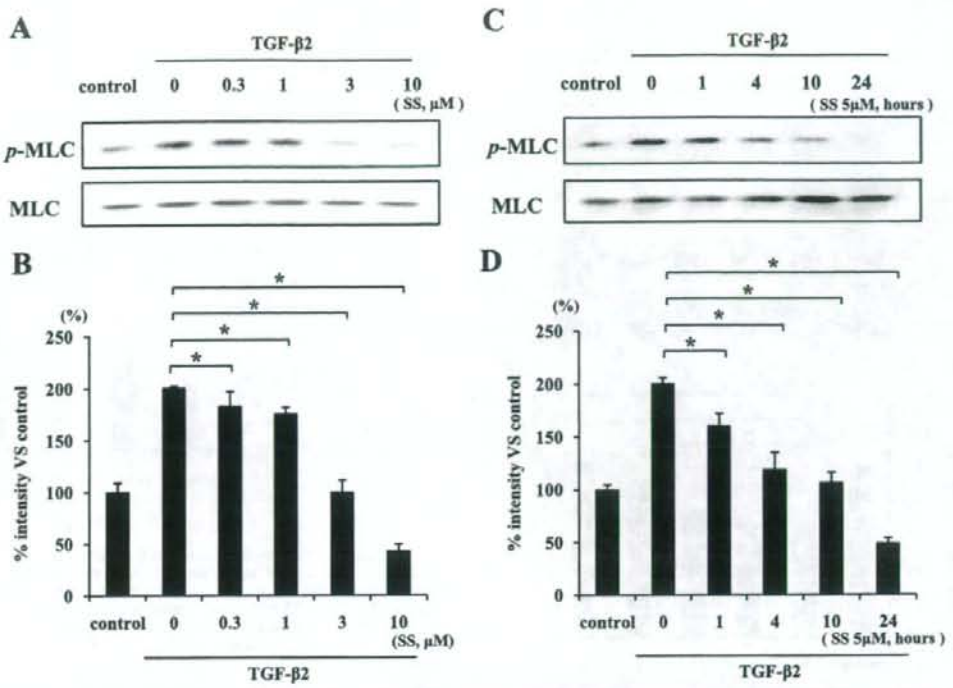

FIG. 2. Inhibitory effect of simvastatin on TGF-β2–dependent MLC phosphorylation. Hyalocytes were starved in Dulbecco's modified Eagle's medium containing 3% calf serum for 24 h. *A*: Hyalocytes were pretreated for 30 min with or without the indicated concentrations of simvastatin (0.3, 1, 3, and 10 μmol/l) and subsequently treated with 3 ng/ml TGF-β2 for 24 h. Total cell lysates were subjected to Western blot analysis with an antibody against *p*-MLC. Lane loading differences were normalized by reblotting the membranes with an antibody against MLC. *C*: Hyalocytes were pretreated with or without 5 μmol/l simvastatin for the indicated time (1, 4, 10, and 24 h) and subsequently treated with 3 ng/ml TGF-β2 for 24 h. *p*-MLC and MLC were also examined in the same way as in Fig. 1*A*. *B* and *D*: Signal intensity ratios (*p*-MLC to MLC) were expressed as percentage of control intensity ratio. **P* < 0.05 compared with TGF-β2 alone.

Heights, IL) detection system. Lane loading differences were normalized by reblotting the membranes with an antibody against MLC (Santa Cruz) (1:1,000).

Plasma membrane proteins from the cells were isolated by Qproteome Plasma Membrane Protein kit (Qiagen, Hilden, Germany) and were subjected to Western blot analysis with an antibody against Rho (1:1,000; Upstate, Charlottesville, VA).

Counting viable cells in collagen gels. After 5 days of treatment, the collagen gels were dissolved by collagenase, and the cell suspension was collected. The viable cell number was counted with hemocytometer after trypan blue staining.

In vivo model of PVR. All experimental procedures using animals adhered to the Association for Research in Vision and Ophthalmology Resolution on the Use of Animals in Ophthalmic and Vision Research. We caused experimental PVR in rabbit eyes as previously described (34). Homologous conjunctival fibroblasts were prepared by harvesting the conjunctival tissue. Twenty eyes from 20 Dutch rabbits weighing 2–2.5 kg were assigned into three groups, and fibroblasts (100,000 cells) were injected into the right eye in each rabbit. Eyes in the first group (six eyes) were administered an intravitreal injection of 0.1 ml vehicle (balanced salt solution). Eyes in the second group (seven eyes) were administered an intravitreal injection of 0.1 ml vehicle containing simvastatin (5 μmol/l final intravitreal concentration). Eyes in the last group (seven eyes) were administered an intravitreal injection of 0.1 ml vehicle containing simvastatin (15 μmol/l final intravitreal concentration). The clinical observations were performed carefully as long as 28 days after surgery and categorized according with the PVR classification of Fastenberg et al. (35).

Electroretinography. Nine eyes from 10 Dutch rabbits weighing 2–2.5 kg were assigned into three groups. Eyes in the first group (three eyes) were administered an intravitreal injection of 0.1 ml vehicle. Eyes in the second group (three eyes) were administered an intravitreal injection of 0.1 ml vehicle containing simvastatin (5 μmol/l final intravitreal concentration). Eyes in the third group (three eyes) were administered an intravitreal injection of 0.1 ml vehicle containing simvastatin (15 μmol/l final intravitreal concentration). Electroretinogram was performed on day 28 as previously described (36).

Light microscopy. The eyes were enucleated and fixed in 4% paraformaldehyde on day 28. Whole eyes were cut approximately along the vertical meridian. Paraffin-embedded sections were stained with hematoxylin-eosin, and each section was examined using light microscopy.

TdT-dUTP terminal nick-end labeling assay. Apoptotic and potentially necrotic cell death was detected by TdT-dUTP terminal nick-end labeling (TUNEL). The eyes were fixed in 4% paraformaldehyde and embedded in paraffin. TUNEL staining was performed with the TdT Fluorescein in situ apoptosis detection kit (R&D Systems), according to the manufacturer's protocols. The sections were costained with propidium iodide (Molecular Probes, Eugene, OR) to observe the cell nuclei by fluorescence microscopy (KEYENCE, BIORAVO, and BZ-9000). As a TUNEL-positive control, we used the retina of rabbit PVR model on day 7 after the onset.

Transmission electron microscopy. The eyes were fixed in 1% glutaraldehyde and 1% paraformaldehyde in PBS. The specimens were postfixed in veronal acetate buffer osmium tetroxide (2%), dehydrated in ethanol and water, and embedded in Epon. Ultrathin sections were cut from blocks and mounted on copper grids. The specimens were observed with an electron microscope (H7650; Hitachi, Tokyo).

Statistical analysis. Statistical differences were assessed using nonparametric test (Kruskal-Wallis variance analysis) for the data of TGF-β2 concentrations and ANOVA for the other groups. *P* values <0.05 were considered significant. To adjust for inflated α-error due to multiple comparisons, the corrected significant *P* value was defined using the Bonferroni correction.

RESULTS

TGF-β2 in the vitreous and its impact on membrane contraction. The median TGF-β2 protein concentrations, 2.35 ng/ml (range 0.72–5.26) in macular hole (n = 27), 4.74 ng/ml (1.60–13.0) in PDR (n = 53), and 4.48 ng/ml (2.52–21.6) in PVR (n = 22) patients, were significantly higher in PDR or PVR patients than in patients with macular hole ($P < 0.01$) (Fig. 1*A*). The median TGF-β2 protein concen-

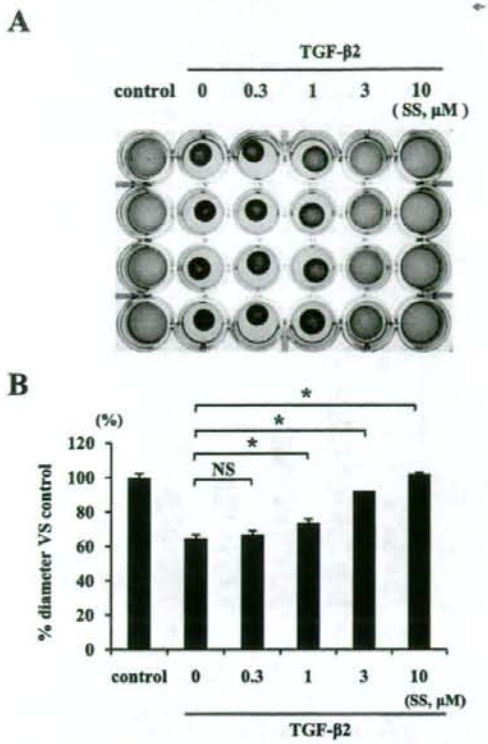

FIG. 3. The effect of simvastatin on TGF-β2–induced contraction of hyalocyte-containing collagen gels. Hyalocytes were embedded in type I collagen gels (n = 4). *A*: After starvation and pretreatment with indicated concentrations of simvastatin for 24 h, the collagen gels were stimulated with 3 ng/ml TGF-β2. Five days after the stimulation, the gels were photographed. *B*: The diameter of the collagen gels was measured and expressed as a percentage of the average diameter of control group. *P < 0.05; NS, not significant compared with TGF-β2 alone.

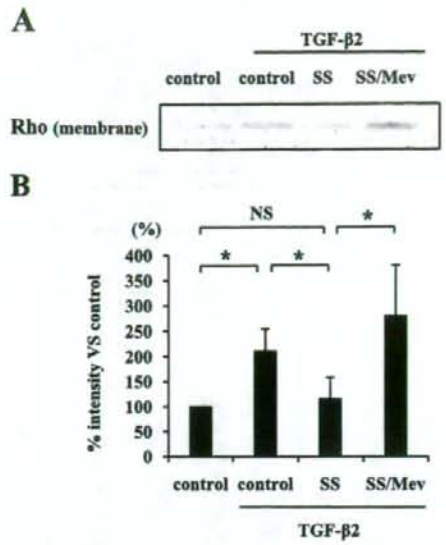

FIG. 4. Inhibitory effect of simvastatin on the Rho translocation to the plasma membrane. *A*: Hyalocytes were pretreated with 5 μmol/l simvastatin with or without mevalonate (Mev) and then treated with 3 ng/ml TGF-β2 for 24 h. Plasma membrane proteins were isolated and subjected to Western blot analysis with an antibody against Rho. *B*: Signal intensities were expressed as percentage of control intensity. *P < 0.05.

tration in the vitreous samples from patients with PDR or PVR showed no significant difference (P = 0.6).

Vitreous samples from patients with PVD and those containing nonspecific IgG induced significant contraction of hyalocyte-containing collagen gels (63 and 67% vs. control, respectively). In comparison, the vitreous-induced contraction was virtually suppressed by specific anti–TGF-β2 antibody (P < 0.05) (97% vs. control) (Fig. 1*B* and *C*), suggesting a key role for TGF-β2 in the vitreous-induced collagen gel contraction.

Role of simvastatin in TGF-β2–dependent MLC phosphorylation. TGF-β2 enhanced MLC phosphorylation to about two times that seen with control (Fig. 2*A* and *B*). TGF-β2–dependent MLC phosphorylation showed a significant reduction at 0.3 μmol/l simvastatin or higher concentrations (up to 10 μmol/l simvastatin) compared with TGF-β2 alone (P < 0.05). The level of MLC phosphorylation at 10 μmol/l simvastatin concentration was lower than in untreated control, suggesting that simvastatin at higher concentrations may block the constitutive level of MLC phosphorylation. Because 3 μmol/l simvastatin was sufficient to reverse the effect of TGF-β2 on MLC phosphorylation, we chose the slightly higher concentration of 5 μmol/l to study the time-dependent effect of simvastatin on TGF-β2–dependent MLC phosphorylation. Treatment of the hyalocytes with 5 μmol/l simvastatin for 1 h or longer (up to 24 h) significantly suppressed the MLC phosphorylation compared with TGF-β2 alone, and treatment with 5 μmol/l simvastatin for 24 h sufficiently suppressed the MLC phosphorylation below that of untreated control (Fig. 2*C* and *D*).

TGF-β2–dependent collagen gel contraction and its inhibition by simvastatin. The control gels showed no apparent contraction up to 5 days, whereas TGF-β2 caused substantial collagen gel contraction in a time-dependent manner in the first 5 days (57.6% vs. control). TGF-β2–dependent collagen gel contraction was significantly reduced by simvastatin starting at a concentration of 1 μmol/l, and the reduction was greater at 3 and 10 μmol/l (92 and 100% vs. control, respectively) (Fig. 3).

TGF-β2–dependent Rho translocation to the plasma membrane and its inhibition by simvastatin. TGF-β2 significantly enhanced the Rho translocation to the plasma membrane (P < 0.05), whereas simvastatin suppressed the translocation (Fig. 4*A* and *B*). However, the effect of simvastatin was reversed in the presence of 400 μmol/l mevalonate, a component of the mevalonate pathway. These findings suggest that simvastatin inhibits Rho/Rho kinase pathway by preventing Rho from translocating to the plasma membrane via inhibition of the mevalonate pathway.

Comparison of the effects of various statins on TGF-β2–dependent MLC phosphorylation and collagen gel contraction. Simvastatin and fluvastatin significantly suppressed TGF-β2–dependent MLC phosphorylation by hyalocytes, whereas pravastatin did not show an effect (Fig. 5*A* and *B*). In addition, simvastatin significantly suppressed MLC phosphorylation compared with fluvastatin (P < 0.05). Next, we compared the inhibitory effect of statins on the contraction of hyalocyte-containing collagen gels. Simvastatin and fluvastatin significantly suppressed TGF-β2–dependent contraction of collagen gel, whereas

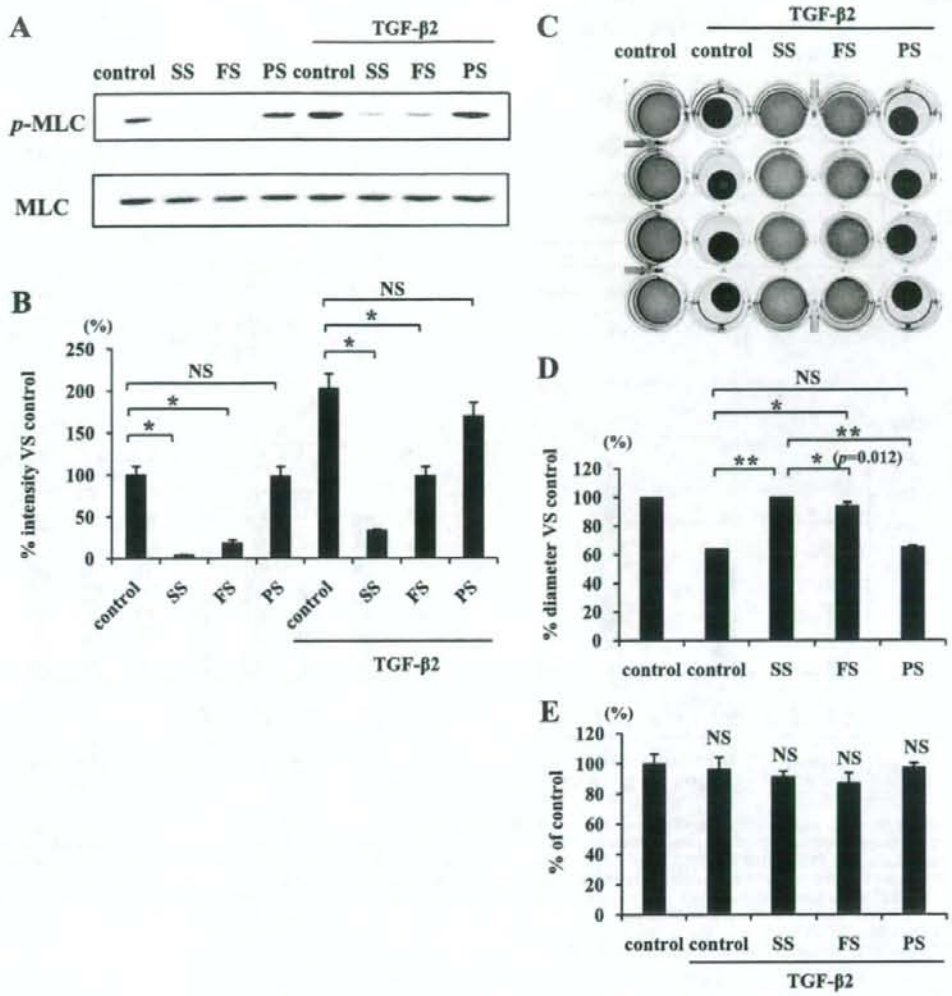

FIG. 5. Comparison of inhibitory effects of simvastatin, fluvastatin, and pravastatin on TGF-β2–dependent MLC phosphorylation and collagen gel contraction. *A*: Starved hyalocytes were pretreated with vehicle, 5 μmol/l simvastatin, fluvastatin, or pravastatin for 30 min and subsequently treated with or without 3 ng/ml TGF-β2 for 24 h. Total cell lysates were subjected to Western blot analysis with an antibody against *p*-MLC. Lane loading differences were normalized by reblotting the membranes with an antibody against MLC. *B*: Signal intensity ratios (*p*-MLC to MLC) were expressed as percentage of intensity ratio of vehicle alone. $^*P < 0.05$. *C*: Hyalocytes were embedded in type I collagen gels ($n = 4$). After starvation and pretreatment with vehicle, 5 μmol/l simvastatin, fluvastatin, or pravastatin for 24 h, the collagen gels were stimulated with 3 ng/ml TGF-β2. Five days after the stimulation, the gels were photographed. *D*: The diameter of the collagen gels was measured and expressed as percentage of the average diameter of control group. $^{**}P < 0.01$, $^*P < 0.05$; NS, not significant. *E*: The viable cell number in the collagen gels was counted to exclude the effect of cell growth or cytotoxicity on the collagen gel contraction or its inhibition. Five days after the treatment, the collagen gels were dissolved, and the cell suspension was collected. The viable cell number was counted with hemocytometer after trypan blue staining ($n = 4$; NS, not significant compared with control).

pravastatin did not show an effect (Fig. 5*C* and *D*). In addition, the inhibitory effect of simvastatin (100% vs. control) was significantly higher than that by fluvastatin (94% vs. control) ($P < 0.05$). To test whether cytokine and/or statin treatment affected the growth and/or viability of the cells in our experiments, we treated the collagen gels with collagenase and counted the number of viable cells. Both TGF-β2 and statins showed no significant effects on cell number in the three-dimensional collagen gels (Fig. 5*E*).

Impact of simvastatin on MLC phosphorylation and collagen gel contraction induced by vitreous samples from patients with PVD. Vitreous samples from patients with PVD caused a significantly larger enhancement of MLC phosphorylation than those from patients with non-PVD (Fig. 6*A* and *B*). Simvastatin (5 μmol/l) strongly attenuated the vitreous-induced MLC phosphorylation. Expression of GAPDH did not change after the treatment with simvastatin or stimulation with vitreous samples. However, total MLC increased in cells stimulated with the vitreous samples compared with cells without vitreous treatment, and the increase was larger in cells stimulated with vitreous samples from patients with PVD than those from patients without PVD. These increases in an amount of total MLC were suppressed by 5 μmol/l simvastatin.

The contraction of hyalocyte-containing collagen gels stimulated with the vitreous samples from patients with PVD was significantly larger compared with the contrac-

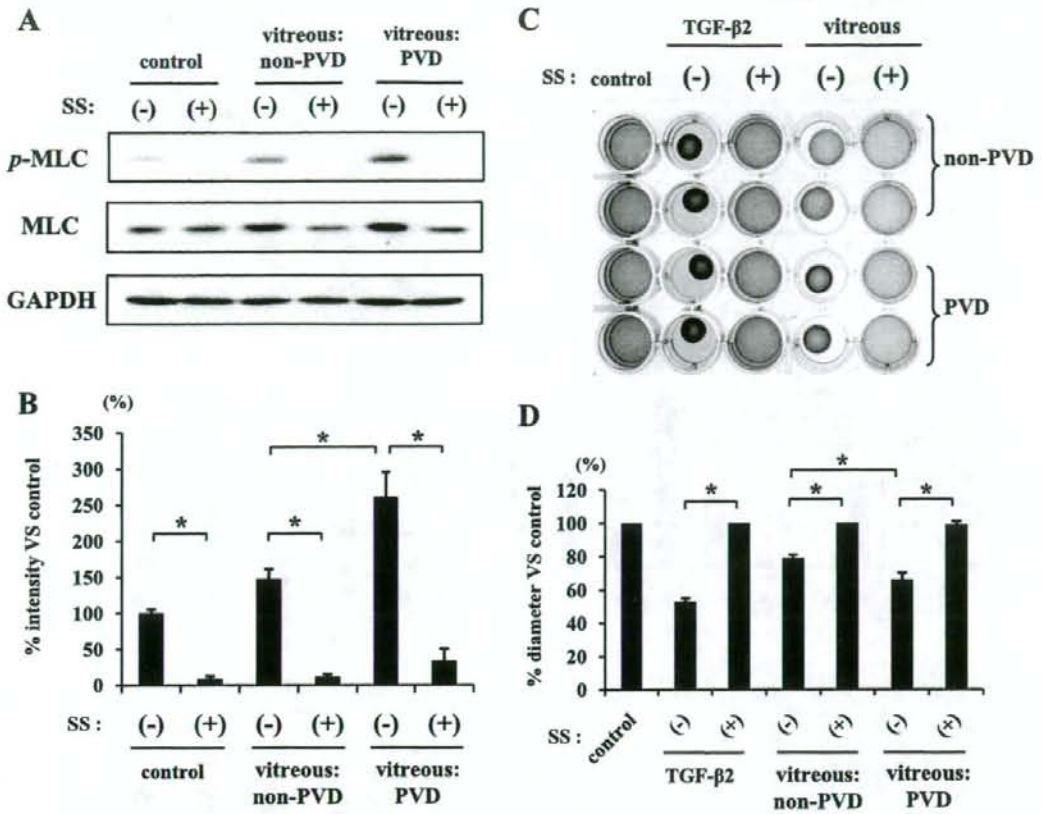

FIG. 6. Inhibitory effects of simvastatin on vitreous-induced MLC phosphorylation and contraction of hyalocyte-containing collagen gels. *A*: Starved hyalocytes were pretreated with 5 μmol/l simvastatin for 30 min and subsequently treated with or without 400 μl vitreous samples of non-PVD (macular hole) or PVD (PDR and PVR) for 24 h. Total cell lysates were subjected to Western blot analysis with an antibody against *p*-MLC. Lane loading differences were normalized by reblotting the membranes with an antibody against MLC and GAPDH. *B*: Signal intensity ratios (*p*-MLC to GAPDH) were expressed as percentage of control intensity ratio. *C*: Hyalocytes were embedded in type I collagen gels ($n = 4$). After starvation and pretreatment with 5 μmol/l simvastatin for 24 h, the collagen gels were stimulated with 400 μl vitreous samples of non-PVD or PVD. Five days after the stimulation, the gels were photographed. *D*: The diameter of the collagen gels was measured and expressed as percentage of the average diameter of the control group. *$P < 0.05$.

tion of the gels stimulated with vitreous samples from patients without PVD ($P < 0.05$) (Fig. 6*C* and *D*). We further examined the inhibitory effect of simvastatin on vitreous-dependent contraction of collagen gels and found that 5 μmol/l simvastatin suppressed the collagen gel contraction induced by vitreous samples even from patients with PVD.

Simvastatin inhibition of PVR development in vivo. The control eyes of rabbits injected with vehicle developed PVR and were accompanied by proliferative membrane formation and cicatricial contraction, resulting in tractional retinal detachment (Fig. 7*A*). In comparison, 5 and 15 μmol/l simvastatin (final intravitreal concentrations) significantly prevented PVR development (Fig. 7*C*). Simvastatin inhibited the contraction of the proliferative membrane, and the membranes in eyes treated with simvastatin were much thinner than those in vehicle-treated eyes (Fig. 7*B*). After simvastatin injections were stopped at day 7, the eyes treated with 5 μmol/l simvastatin developed a mild but significant PVR, whereas no significant PVR development was observed in the eyes treated with 15 μmol/l simvastatin.

Absence of apparent adverse effects of simvastatin in the retina. To evaluate the retinal function after intravitreal application of simvastatin, we performed electroretinography. The mean amplitude and latency of the 2Hz b wave in the eyes treated with 5 or 15 μmol/l simvastatin were 203.4 μV and 28.1 ms and 201.7 μV and 28.4 ms, respectively, and were not significantly different from those without any treatment or those of the vehicle-treated eyes (204.8 μV and 28.1 ms), suggesting that at these concentrations, simvastatin may not impede retinal function (Fig. 8*A*).

The histological structure of the retina in the eyes injected with simvastatin appeared normal when observed on day 28 (Fig. 8*B*, C).

In the retina of an experimental PVR used as a positive-control, apoptotic cells, which present TUNEL-positive staining (green), were detected in the inner nuclear layer and the outer nuclear layer (Fig. 8*D*). The eyes injected with simvastatin had no apparent TUNEL-positive staining in the retina when observed on day 28 (Fig. 8*E*).

The eyes injected with simvastatin had no apparent ultrastructual changes in internal limiting membrane,

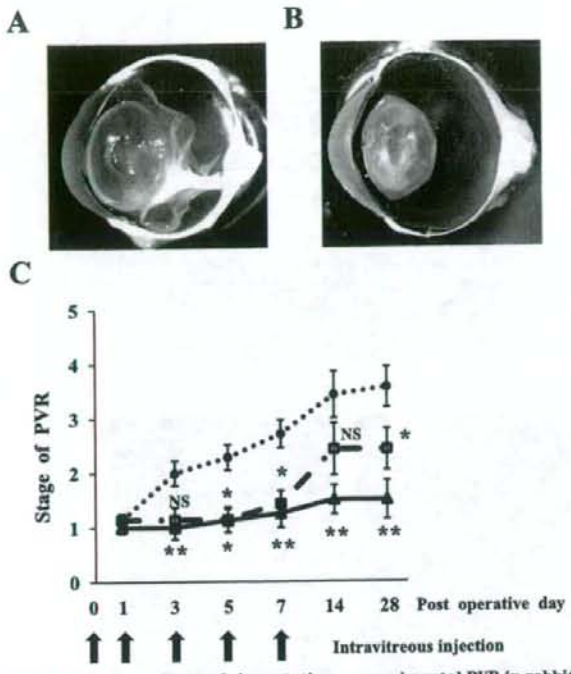

FIG. 7. Inhibitory effects of simvastatin on experimental PVR in rabbit eyes. Rabbits underwent vitrectomy and intravitreal injection of fibroblasts with and without simvastatin on day 0. The eyes were injected with same contents of simvastatin on days 1, 3, 5, and 7 and examined using indirect ophthalmoscope as long as 28 days after the surgery. *A*: A representative vehicle-injected eye with PVR in stage 5, 28 days after the surgery. Proliferative membranes were observed in the vitreous cavity, causing a traction to the retina and retinal detachment. *B*: A representative simvastatin-injected eye (15 μmol/l) with PVR in stage 1. A thin proliferative membrane was observed, however, there was no evidence of tractional retinal detachment. *C*: Clinical observations were categorized according to the PVR classification of Fastenberg et al. (35). Stage 1, intravitreal membrane; stage 2, focal traction, localized vascular changes, hyperemia, engorgement, dilation, and blood vessel elevation; stage 3, localized detachment of medullary ray; stage 4, extensive retinal detachment, total medullary ray detachment, and peripapillary retinal detachment; and stage 5, total retinal detachment. ●, vehicle; □, 5 μmol/l simvastatin; ▲, 15 μmol/l simvastatin. **P < 0.01, *P < 0.05; NS, not significant compared with vehicle.

nerve fiber layer, and ganglion cell layer (Fig. 8*G*) compared with the untreated control eyes (Fig. 8*F*). In other parts of the retina, such as inner and outer nuclear layers, photoreceptors, and retinal pigment epitheliums, there were also no apparent changes.

DISCUSSION

Blindness is a devastating consequence of PVDs such as PDR and PVR. Currently, the progression of these diseases cannot be effectively prevented, and the treatment options are limited to vitreoretinal surgery. An effective pharmacological treatment is thus urgently needed to complement or potentially replace the surgical intervention. In the current study, we show statins' novel function in inhibiting the Rho/Rho-kinase pathway, the contraction of collagen gel, and the progression of experimental PVR, suggesting the therapeutic potential of these compounds for the treatment of PVDs.

Various cytokines, such as TGF-β, connective tissue growth factor, interleukin-6, and platelet-derived growth factor (PDGF), are overexpressed in the vitreous and membranes associated with PDR and PVR, and they contribute to the pathogenesis of these diseases (15,37–40). Among these cytokines, TGF-β2 induces the transformation of retinal pigment epithelial cells or hyalocytes to myofibroblastic cells (18,41) and plays a key role in the formation and contraction of proliferative membranes. In this study, we confirmed the overexpression of TGF-β2 in the vitreous from patients with PVD (PDR and PVR) and showed that TGF-β2 inhibition strongly suppressed the vitreous-induced contraction of the collagen gels. This indicates the possibility that TGF-β2 is the dominant contributor to the contraction of proliferative membrane in the vitreous cavity. Thus, we focused on the role of TGF-β2 to investigate the mechanisms of membrane contraction. TGF-β2 enhanced MLC phosphorylation in hyalocytes that was responsible for the contraction of the hyalocyte-containing collagen gels. We showed that simvastatin suppressed TGF-β2–induced MLC phosphorylation and collagen gel contraction in a dose-dependent fashion by inhibiting GGPP-mediated translocation of Rho to the plasma membrane, whereas no signs of cytotoxicity were apparent.

Differences in the structural characteristics of statin cause different levels of lipophilicity and possibly of efficacies and also cytotoxicity. Pravastatin is strongly hydrophilic, and simvastatin is much more lipophilic than pravastatin (42). Fluvastatin is also more lipophilic than pravastatin; however, it is less lipophilic than simvastatin (43). Although our comparison of the inhibitory effects of various statins, simvastatin, fluvastatin, and pravastatin, revealed that simvastatin was more effective in reducing MLC phosphorylation than the other statins under the chosen experimental conditions, the results might vary at other time points or concentrations. Further examination is necessary to determine the order. Additionally, because cerivastatin is more lipophilic than simvastatin (44), we studied the effects of cerivastatin and simvastatin. Many hyalocytes treated with 5 μmol/l cerivastatin for 24 h shrank and detached from the culture plates, whereas the cells treated with 5 μmol/l simvastatin remained morphologically unchanged. However, at higher concentrations (>20 μmol/l), some hyalocyte shrinkage was observed even with simvastatin (data not shown). Cerivastatin is known to be cytotoxic and induce apoptosis (45). The morphological changes we observed in cerivastatin-treated hyalocytes in our study suggest that this drug may also be toxic to hyalocytes and promote their apoptosis. Because the lipophilicity of lovastatin is similar to that of simvastatin (42), we compared their effect and found the inhibitory effect of simvastatin on MLC phosphorylation and collagen gel contraction to be greater than that of 5 μmol/l lovastatin for 24 h (data not shown).

Vitreous samples from patients with PDR and PVR induced MLC phosphorylation and contraction of hyalocyte-containing collagen gels, which were effectively inhibited by simvastatin. It may appear surprising that not only vitreous samples from patients with PVD but also those from non-PVD patients induced MLC phosphorylation and collagen gel contraction. However, this might be explained by the fact that TGF-β2 is expressed in vitreous samples of patients with macular hole at high enough concentrations to induce the observed phenomena. The concentrations of TGF-β2 in vitreous samples from patients with PVD (PDR and PVR) were higher than in those from macular hole patients. Therefore, in a concentration-dependent manner, the inductions might be greater in the vitreous samples

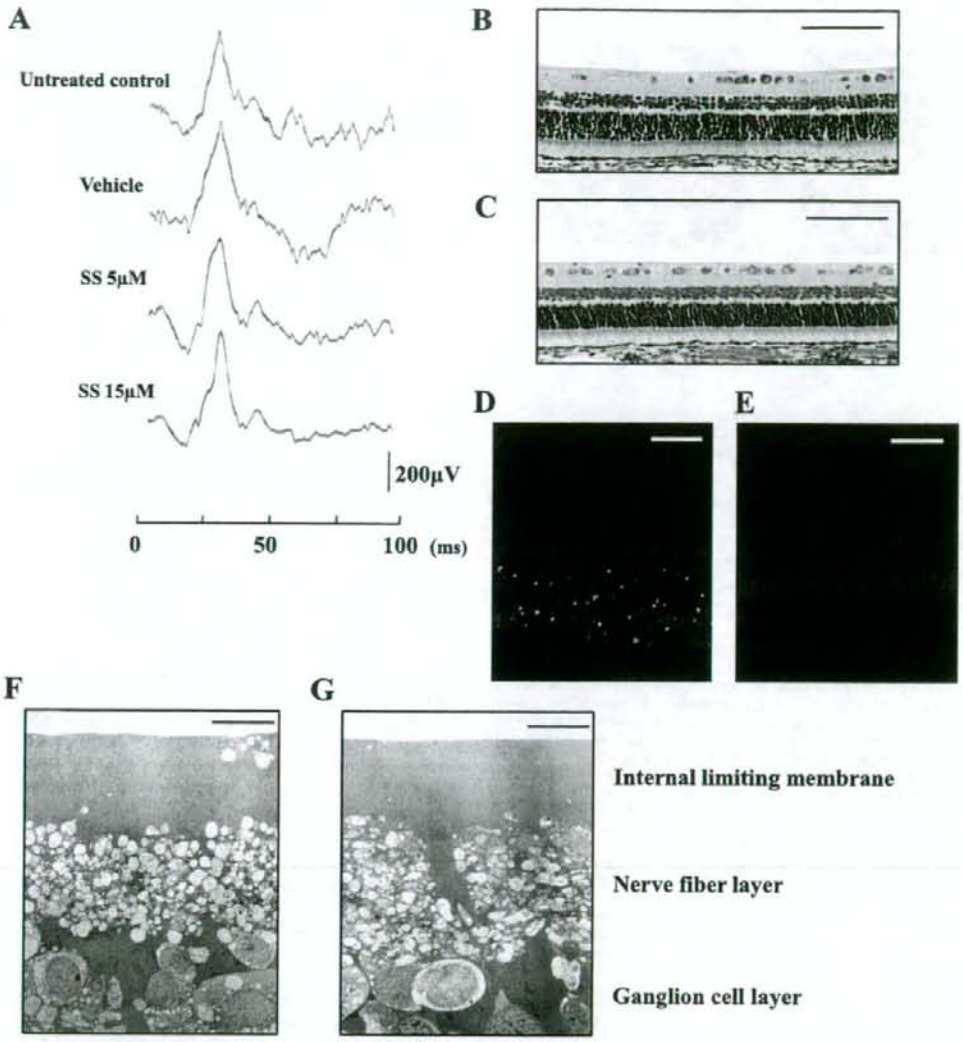

FIG. 8. Histological and physiological examinations of eyes injected with simvastatin. Rabbits received intravitreal injections of 0.1 ml vehicle or vehicle with simvastatin (final concentration of 5 or 15 μmol/l simvastatin) on days 0, 1, 3, 5, and 7. *A*: Electroretinograms on day 28. A flash stimulus of intensity 1.30 log cd.s/m^2 was superimposed on a background luminance of 1.15 log cd/m^2. Light microscopy of the rabbit eye without any treatment (*B*) and that of the eye injected with 15 μmol/l simvastatin (*C*). Scale bar = 100 μm. Apoptotic and potentially necrotic cell death detected by TUNEL in the section from positive control (rabbit PVR model on day 7 after its onset) (*D*) and in the section from the 15 μmol/l simvastatin-treated eye (*E*). Scale bar = 50 μm. Transmission electron microscopy of the rabbit eye without treatment (*F*) and that of the eye injected with 15 μmol/l simvastatin (*G*). Scale bar = 10 μm. (Please see http://dx.doi.org/10.2337/db08-0302 for a high-quality digital representation of this image.)

from patients with PVD than in those from patients without PVD. The concentrations of TGF-β2 in some vitreous samples from patients with macular hole were higher than those with PDR and PVR. However, the pathology of macular hole does not generally involve proliferative membrane formation and tractional retinal detachment. Occasionally, epiretinal membranes and retinal folds accompany macular hole. Retinal folds are considered to be caused by the contraction of the epiretinal membranes. TGF-β2 concentrations in vitreous samples from patients with macular hole may be high enough to induce contraction of proliferative membranes, however, because the epiretinal membrane in these patients does not extend into the vitreous and is very thin; the expression of TGF-β2 remains inconsequential.

MLC phosphorylation depends on the concentration of TGF-β2 (18); thus, the eyes with PVR having lower TGF-β2 concentrations might represent a less severe pathology, or remission, compared with those with higher TGF-β2 concentrations. The occurrence of tractional retinal detachment might depend on the presence or absence of proliferative membranes and the concentration of TGF-β2.

Although TGF-β2–stimulated hyalocytes showed no significant change in MLC expression, those stimulated with vitreous samples showed elevated MLC expression that was inhibited by simvastatin treatment. The vitreous in-

cludes various cytokines, released from retinal pigment epithelial cells, glial cells, macrophages, and other intravitreal cells (46). Thus, some cytokines other than TGF-β2 might elevate the expression of MLC. Among the cytokines found in the vitreous, insulin-like growth factor-I (IGF-I), PDGF, and members of the endothelin family have been shown to stimulate extracellular matrix contraction (18,47,48). This study reveals a key role for TGF-β2 in the pathology of PVDs; however, it is possible that other cytokines found in the vitreous might also be involved in MLC phosphorylation and contraction of hyalocyte-containing collagen gels. Because simvastatin almost completely inhibited the phenomena induced by vitreous samples, it might also inhibit the effect of the other cytokines, such as IGF-I, PDGF, and members of the endothelin family and unknowns, which might be exerted through the Rho/Rho-kinase pathway.

Simvastatin also prevented the development of PVR in vivo. Proliferative membranes in simvastatin-injected eyes, even if present, were very thin, whereas the membranes in vehicle injected eyes with PVR in stage 4 or 5 were thick. Thus, simvastatin might have also an inhibitory effect on the formation and growth of proliferative membranes in addition to the cicatricial contraction of proliferative membranes. However, after the end of the simvastatin injections, even in the groups treated with higher concentration of simvastatin (15 μmol/l) the development of PVR was not completely inhibited. This may be due to a short biological half-life time of the compound in the vitreous cavity. Therefore, to sustain a constant level of intravitreal simvastatin concentration, frequent injections or a slow release drug delivery system might be necessary.

Recent findings suggest that statins might have a number of beneficial effects in the eye. Although the applicability of statins on age-related macular degeneration is still under investigation (49), statins are shown to have protective effects on primary open-angle glaucoma, a major cause of blindness (50). The regulation of the intraocular pressure (IOP) within a physiological range is of great clinical importance. Statins are reported to downregulate the IOP by increasing aqueous humor outflow via the inhibition of Rho/Rho-kinase pathway in the trabecular meshwork and the ciliary body (50).

In conclusion, simvastatin potently inhibits the Rho/Rho-kinase pathway and thus might have therapeutic potential in the prevention of cicatricial contraction of proliferative membranes in vivo. This is the first report demonstrating the beneficial effects of simvastatin in inhibiting the development of PVR. Statins might provide a new strategy for the treatment and prevention of the development of PVDs in humans.

ACKNOWLEDGMENTS

S.N. has received a Research Fellowship Award from Bausch & Lomb and a Fellowship Award from the Japan Eye Bank Association. A.H.-M. has received National Institutes of Health Grants AI050775 and HL086933. This study has received Grants-in-Aid for Scientific Research 19592026, 18791283, and 18591925 from the Ministry of Education, Science, Sports and Culture, Japan; National Eye Institute Core Grant EY14104; and support from the Massachusetts Lions Eye Research Fund, the Marion W. and Edward F. Knight Age-Related and Macular Degeneration Fund, and Research to Prevent Blindness.

We acknowledge David Goodman (Pharmascience), Waichiro Katsuda, Tomoko Saeki, and Noriyuki Yoshida (Aqumen Biopharmaceuticals) for their excellent help.

REFERENCES

1. Pastor JC, de la Rua ER, Martin F: Proliferative vitreoretinopathy: risk factors and pathobiology. *Prog Retin Eye Res* 21:127–144, 2002
2. Pastor JC: Proliferative vitreoretinopathy: an overview. *Surv Ophthalmol* 43:3–18, 1998
3. Friedlander M: Fibrosis and diseases of the eye. *J Clin Invest* 117:576–586, 2007
4. Campochiaro PA: Pathogenic mechanisms in proliferative vitreoretinopathy. *Arch Ophthalmol* 115:237–241, 1997
5. Jerdan JA, Pepose JS, Michels RG, Hayashi H, de Bustros S, Sebag M, Glaser BM: Proliferative vitreoretinopathy membranes: an immunohistochemical study. *Ophthalmology* 96:801–810, 1989
6. Vinores SA, Campochiaro PA, Conway BP: Ultrastructural and electron-immunocytochemical characterization of cells in epiretinal membranes. *Invest Ophthalmol Vis Sci* 31:14–28, 1990
7. Machemer R, Laqua H: Pigment epithelium proliferation in retinal detachment (massive periretinal proliferation). *Am J Ophthalmol* 80:1–23, 1975
8. Lazarus HS, Hageman GS: In situ characterization of the human hyalocyte. *Arch Ophthalmol* 112:1356–1362, 1994
9. Grabner G, Boltz G, Forster O: Macrophage-like properties of human hyalocytes. *Invest Ophthalmol Vis Sci* 19:333–340, 1980
10. Mitchell CA, Risau W, Drexler HC: Regression of vessels in the tunica vasculosa lentis is initiated by coordinated endothelial apoptosis: a role for vascular endothelial growth factor as a survival factor for endothelium. *Dev Dyn* 213:322–333, 1998
11. Kampik A, Kenyon KR, Michels RG, Green WR, de la Cruz ZC: Epiretinal and vitreous membranes: comparative study of 56 cases. *Arch Ophthalmol* 99:1445–1454, 1981
12. Faulborn J, Dunker S, Bowald S: Diabetic vitreopathy: findings using the celloidin embedding technique. *Ophthalmologica* 212:369–376, 1998
13. Pfeffer BA, Flanders KC, Guerin CJ, Danielpour D, Anderson DH: Transforming growth factor beta 2 is the predominant isoform in the neural retina, retinal pigment epithelium-choroid and vitreous of the monkey eye. *Exp Eye Res* 59:323–333, 1994
14. Connor TB Jr, Roberts AB, Sporn MB, Danielpour D, Dart LL, Michels RG, de Bustros S, Enger C, Kato H, Lansing M: Correlation of fibrosis and transforming growth factor-beta type 2 levels in the eye. *J Clin Invest* 83:1661–1666, 1989
15. Kita T, Hata Y, Kano K, Miura M, Nakao S, Noda Y, Shimokawa H, Ishibashi T: Transforming growth factor-β2 and connective tissue growth factor in proliferative vitreoretinal diseases: possible involvement of hyalocytes and therapeutic potential of Rho kinase inhibitor. *Diabetes* 56:231–238, 2007
16. Ando A, Ueda M, Uyama M, Masu Y, Ito S: Enhancement of dedifferentiation and myoid differentiation of retinal pigment epithelial cells by platelet derived growth factor. *Br J Ophthalmol* 84:1306–1311, 2000
17. Vinores SA, Henderer JD, Mahlow J, Chiu C, Derevjanik NL, Larochelle W, Csaky C, Campochiaro PA: Isoforms of platelet-derived growth factor and its receptors in epiretinal membranes: immunolocalization to retinal pigmented epithelial cells. *Exp Eye Res* 60:607–619, 1995
18. Hirayama K, Hata Y, Noda Y, Miura M, Yamanaka I, Shimokawa H, Ishibashi T: The involvement of the rho-kinase pathway and its regulation in cytokine-induced collagen gel contraction by hyalocytes. *Invest Ophthalmol Vis Sci* 45:3896–3903, 2004
19. Jester JV, Ho-Chang J: Modulation of cultured corneal keratocyte phenotype by growth factors/cytokines control in vitro contractility and extracellular matrix contraction. *Exp Eye Res* 77:581–592, 2003
20. Molgaard J, von Schenck H, Olsson AG: Effects of simvastatin on plasma lipid, lipoprotein and apolipoprotein concentrations in hypercholesterolaemia. *Eur Heart J* 9:541–551, 1988
21. Graaf MR, Richel DJ, van Noorden CJ, Guchelaar HJ: Effects of statins and farnesyltransferase inhibitors on the development and progression of cancer. *Cancer Treat Rev* 30:609–641, 2004
22. MRC/BHF Heart Protection Study of cholesterol lowering with simvastatin in 20,536 high-risk individuals: a randomised placebo-controlled trial. *Lancet* 360:7–22, 2002
23. Coons JC: Hydroxymethylglutaryl-coenzyme A reductase inhibitors in osteoporosis management. *Ann Pharmacother* 36:326–330, 2002
24. Campbell MJ, Esserman LJ, Zhou Y, Shoemaker M, Lobo M, Borman E, Baehner F, Kumar AS, Adduci K, Marx C, Petricoin EF, Liotta LA, Winters M, Benz S, Benz CC: Breast cancer growth prevention by statins. *Cancer Res* 66:8707–8714, 2006

25. Matar P, Rozados VR, Binda MM, Roggero EA, Bonfil RD, Scharovsky OG: Inhibitory effect of Lovastatin on spontaneous metastases derived from a rat lymphoma. *Clin Exp Metastasis* 17:19–25, 1999
26. Van Aelst L, D'Souza-Schorey C: Rho GTPases and signaling networks. *Genes Dev* 11:2295–2322, 1997
27. Laufs U, Liao JK: Post-transcriptional regulation of endothelial nitric oxide synthase mRNA stability by Rho GTPase. *J Biol Chem* 273:24266–24271, 1998
28. Hall A: Rho GTPases and the actin cytoskeleton. *Science* 279:509–514, 1998
29. Paterson HF, Self AJ, Garrett MD, Just I, Aktories K, Hall A: Microinjection of recombinant p21rho induces rapid changes in cell morphology. *J Cell Biol* 111:1001–1007, 1990
30. Takaishi K, Sasaki T, Kato M, Yamochi W, Kuroda S, Nakamura T, Takeichi M, Takai Y: Involvement of Rho p21 small GTP-binding protein and its regulator in the HGF-induced cell motility. *Oncogene* 9:273–279, 1994
31. Kureishi Y, Kobayashi S, Amano M, Kimura K, Kanaide H, Nakano T, Kaibuchi K, Ito M: Rho-associated kinase directly induces smooth muscle contraction through myosin light chain phosphorylation. *J Biol Chem* 272:12257–12260, 1997
32. Amano M, Chihara K, Kimura K, Fukata Y, Nakamura N, Matsuura Y, Kaibuchi K: Formation of actin stress fibers and focal adhesions enhanced by Rho-kinase. *Science* 275:1308–1311, 1997
33. Noda Y, Hata Y, Hisatomi T, Nakamura Y, Hirayama K, Miura M, Nakao S, Fujisawa K, Sakamoto T, Ishibashi T: Functional properties of hyalocytes under PDGF-rich conditions. *Invest Ophthalmol Vis Sci* 45:2107–2114, 2004
34. Dong X, Chen N, Xie L, Wang S: Prevention of experimental proliferative vitreoretinopathy with a biodegradable intravitreal drug delivery system of all-trans retinoic acid. *Retina* 26:210–213, 2006
35. Fastenberg DM, Diddie KR, Dorey K, Ryan SJ: The role of cellular proliferation in an experimental model of massive periretinal proliferation. *Am J Ophthalmol* 93:565–572, 1982
36. Ito S, Sakamoto T, Tahara Y, Goto Y, Akazawa K, Ishibashi T, Inomata H: The effect of tranilast on experimental proliferative vitreoretinopathy. *Graefes Arch Clin Exp Ophthalmol* 237:691–696, 1999
37. Robbins SG, Mixon RN, Wilson DJ, Hart CE, Robertson JE, Westra I, Planck SR, Rosenbaum JT: Platelet-derived growth factor ligands and receptors immunolocalized in proliferative retinal diseases. *Invest Ophthalmol Vis Sci* 35:3649–3663, 1994
38. Hinton DR, Spee C, He S, Weitz S, Usinger W, LaBree L, Oliver N, Lim JI: Accumulation of NH_2-terminal fragment of connective tissue growth factor in the vitreous of patients with proliferative diabetic retinopathy. *Diabetes Care* 27:758–764, 2004
39. Hinton DR, He S, Jin ML, Barron E, Ryan SJ: Novel growth factors involved in the pathogenesis of proliferative vitreoretinopathy. *Eye* 16:422–428, 2002
40. Kauffmann DJ, van Meurs JC, Mertens DA, Peperkamp E, Master C, Gerritsen ME: Cytokines in vitreous humor: interleukin-6 is elevated in proliferative vitreoretinopathy. *Invest Ophthalmol Vis Sci* 35:900–906, 1994
41. Gamulescu MA, Chen Y, He S, Spee C, Jin M, Ryan SJ, Hinton DR: Transforming growth factor beta2-induced myofibroblastic differentiation of human retinal pigment epithelial cells: regulation by extracellular matrix proteins and hepatocyte growth factor. *Exp Eye Res* 83:212–222, 2006
42. Serajuddin AT, Ranadive SA, Mahoney EM: Relative lipophilicities, solubilities, and structure-pharmacological considerations of 3-hydroxy-3-methylglutaryl-coenzyme A (HMG-CoA) reductase inhibitors pravastatin, lovastatin, mevastatin, and simvastatin. *J Pharm Sci* 80:830–834, 1991
43. Hamelin BA, Turgeon J: Hydrophilicity/lipophilicity: relevance for the pharmacology and clinical effects of HMG-CoA reductase inhibitors. *Trends Pharmacol Sci* 19:26–37, 1998
44. Chauhan NB, Siegel GJ, Feinstein DL: Effects of lovastatin and pravastatin on amyloid processing and inflammatory response in TgCRND8 brain. *Neurochem Res* 29:1897–1911, 2004
45. Kobayashi M, Kaido F, Kagawa T, Itagaki S, Hirano T, Iseki K: Preventive effects of bicarbonate on cerivastatin-induced apoptosis. *Int J Pharm* 341:181–188, 2007
46. El-Ghrably IA, Dua HS, Orr GM, Fischer D, Tighe PJ: Intravitreal invading cells contribute to vitreal cytokine milieu in proliferative vitreoretinopathy. *Br J Ophthalmol* 85:461–470, 2001
47. Guidry C, Hook M: Endothelins produced by endothelial cells promote collagen gel contraction by fibroblasts. *J Cell Biol* 115:873–880, 1991
48. Guidry C: Tractional force generation by porcine Muller cells: development and differential stimulation by growth factors. *Invest Ophthalmol Vis Sci* 38:456–468, 1997
49. Wilson HL, Schwartz DM, Bhatt HR, McCulloch CE, Duncan JL: Statin and aspirin therapy are associated with decreased rates of choroidal neovascularization among patients with age-related macular degeneration. *Am J Ophthalmol* 137:615–624, 2004
50. Song J, Deng PF, Stinnett SS, Epstein DL, Rao PV: Effects of cholesterol-lowering statins on the aqueous humor outflow pathway. *Invest Ophthalmol Vis Sci* 46:2424–2432, 2005

The American Journal of Pathology, Vol. 173, No. 5, November 2008

DOI: 10.2353/ajpath.2008.080466

Cell Injury, Repair, Aging and Apoptosis

Inhibition of Nuclear Translocation of Apoptosis-Inducing Factor Is an Essential Mechanism of the Neuroprotective Activity of Pigment Epithelium-Derived Factor in a Rat Model of Retinal Degeneration

Yusuke Murakami,*† Yasuhiro Ikeda,† Yoshikazu Yonemitsu,‡ Mitsuho Onimaru,* Kazunori Nakagawa,* Ri-ichiro Kohno,† Masanori Miyazaki,† Toshio Hisatomi,† Makoto Nakamura,§ Takeshi Yabe,¶ Mamoru Hasegawa,‖ Tatsuro Ishibashi,† and Katsuo Sueishi*

From the Department of Pathology, Division of Pathophysiological and Experimental Pathology, and the Department of Ophthalmology,† Graduate School of Medical Sciences, Kyushu University, Fukuoka; the Department of Gene Therapy,‡ Chiba University Graduate School of Medicine, Chiba; the Department of Organs Therapeutics,§ Division of Ophthalmology, Kobe University Graduate School of Medicine, Kobe; the Kitasato Institute for Life Sciences,¶ Kitasato University, Tokyo; and DNAVEC Corporation,‖ Ibaraki, Japan*

Photoreceptor apoptosis is a critical process of retinal degeneration in retinitis pigmentosa (RP), a group of retinal degenerative diseases that result from rod and cone photoreceptor cell death and represent a major cause of adult blindness. We previously demonstrated the efficient prevention of photoreceptor apoptosis by intraocular gene transfer of pigment epithelium-derived factor (PEDF) in animal models of RP; however, the underlying mechanism of the neuroprotective activity of PEDF remains elusive. In this study, we show that an apoptosis-inducing factor (AIF)-related pathway is an essential target of PEDF-mediated neuroprotection. PEDF rescued serum starvation-induced apoptosis, which is mediated by AIF but not by caspases, of R28 cells derived from the rat retina by preventing translocation of AIF into the nucleus. Nuclear translocation of AIF was also observed in the apoptotic photoreceptors of Royal College of Surgeons rats, a well-known animal model of RP that carries a mutation of the *Mertk* gene. Lentivirus-mediated retinal gene transfer of PEDF prevented the nuclear translocation of AIF *in vivo*, resulting in the inhibition of the apoptotic loss of their photoreceptors in association with up-regulated Bcl-2 expression, which mediates the mitochondrial release of AIF. These findings clearly demonstrate that AIF is an essential executioner of photoreceptor apoptosis in inherited retinal degeneration and provide a therapeutic rationale for PEDF-mediated neuroprotective gene therapy for individuals with RP. *(Am J Pathol 2008, 173:1326–1338; DOI: 10.2353/ajpath.2008.080466)*

Retinitis pigmentosa (RP) is a group of retinal degenerative diseases resulting from rod and cone photoreceptor cell death, and a major cause of blindness in adults. RP is caused by mutation in various genes expressed in photoreceptors, the retinal pigment epithelium (RPE) and choriocapillaris of the eye[1,2]; on the other hand, photoreceptors undergo a common mode of cell death, apoptosis.[3,4] Despite extensive efforts to better understand and treat RP, the mechanisms underlying the photoreceptor apoptosis are still unclear and these diseases remain intractable.

Supported in part by the Japanese Ministry of Education, Culture, Sports, Science, and Technology (grants-in-aid 16390118, 17689047, and 19209012 to Y.I., Y.Y., and K.S.).

Accepted for publication August 7, 2008.

Competing Interest Statement: Y.Y. is a member of the Scientific Advisory Board of DNAVEC Corporation.

Supplemental material for this article can be found on *http://ajp.amjpathol.org*.

Address reprint requests to Katsuo Sueishi, M.D., Ph.D., Division of Pathophysiological and Experimental Pathology, Department of Pathology, Graduate School of Medical Sciences, Kyushu University, 3-1-1 Maidashi, Higashi-ku, Fukuoka, 812-8582, Japan. E-mail: sueishi@pathol1.med.kyushu-u.ac.jp.

Pigment epithelium-derived factor (PEDF) is a 50-kDa secreted glycoprotein that was isolated from the conditioned medium of human RPE,[5,6] and shows both neuroprotective and anti-angiogenic properties.[7,8] Vitreous samples from patients with RP contain significantly lower levels of PEDF than those from patients with other retinal conditions.[9] We previously demonstrated that a lentiviral vector based on the simian immunodeficiency virus from African green monkeys (SIVagm) showed sustained transgene expression in RPE of the rat retina,[10] and SIV-mediated retinal gene transfer of PEDF efficiently prevented photoreceptor apoptosis in Royal College of Surgeons (RCS) rats, an animal model of retinal degeneration caused by a *Mertk* mutation.[11] In addition, these protective effects of PEDF have also been observed in rds mice (M. Miyazaki et al, unpublished observations) and rd1 mice,[12] in which the deficits of photoreceptors are caused by different mutations, suggesting the possibility that PEDF might suppress a common pathway leading to the photoreceptor apoptosis. Several studies have demonstrated the direct protective effects on neuronal cells in culture,[13] but the precise mechanism by which PEDF acts on photoreceptors remains unknown.

The caspase family has emerged as a central regulator of apoptosis, especially in the developmental stages. However, recent evidence indicates that apoptosis can be induced by a caspase-independent pathway in several pathological states.[14] Apoptosis-inducing factor (AIF), a flavoprotein in the mitochondrial intermembrane space, has been identified as a caspase-independent apoptotic inducer,[15,16] and plays a prosurvival role through its redox activity under normal conditions.[17,18] AIF translocates to the nucleus during the apoptotic process, and causes peripheral chromatin condensation and large-scale fragmentation of DNA.[19,20] The translocation of AIF has been implicated in several types of neuronal demise, including photoreceptor apoptosis, and has been shown to contribute significantly to the apoptotic process.[21–23]

In the present study, we investigated the signaling pathways related to photoreceptor apoptosis that could be targets of the neuroprotective activity of PEDF *in vitro* and *in vivo*. We found that the nuclear translocation of AIF occurs in apoptotic photoreceptors in RCS rats, and that PEDF targets this process, resulting in the prevention of the apoptosis.

Materials and Methods

Reagents and SIV Vectors

The recombinant human (rhPEDF) was prepared as previously described.[24] His-tagged rhPEDF cloned into pCEP4 vector was isolated from medium conditioned by HEK293 cells. Polyclonal anti-hPEDF antibody was purchased from R&D Systems (Minneapolis, MN). The broad range caspase inhibitor Z-VAD-fmk was obtained from Peptide Institute (Osaka, Japan). Staurosporine was from Alomone Labs (Jerusalem, Israel). To produce third-generation recombinant SIVagm-based lentiviral vectors, HEK293T cells were transfected with the packaging vector, the gene transfer vectors encoding hPEDF (SIV-hPEDF) driven by the cytomegalovirus promoter, the Rev expression vector, and the envelope vector, pVSV-G (Clontech Laboratories, Inc., Mountain View, CA). The SIV vector lacking a transgene cassette (SIV-Empty) was used as the control vector. A U3 region in the 3′ and 5′ long terminal repeat of the SIVagm was deleted to induce self-inactivation. The virus titer was determined by a transduction of the HEK293T cells as expressed in transducing Us/ml, and these viruses were kept at −80°C until just before use.

Cell Culture and Viability Assay

R28 cells, an immortalized retinal precursor cell line derived from the rat retina at postnatal day 6, were the kind gift of Gail M. Seigel (The State University of New York, Buffalo, NY). R28 cells were cultured in Dulbecco's modified Eagle's medium-high glucose with 10% fetal bovine serum, 1× minimum essential medium, 1 × 10 mmol/L nonessential amino acids, 0.37% sodium bicarbonate, and 10 mg/ml gentamicin (Invitrogen, Carlsbad, CA). To induce cell death by serum starvation, R28 cells at 50% confluence were washed with phosphate-buffered saline (PBS) twice, and the culture medium was replaced with 100 μl of serum-free medium. After 6 hours for synchronization, rhPEDF or PBS was added to each well at the indicated concentration. After incubation for 48 hours, the cell viability was assessed by a Cell Counting Kit-8 (Dojindo Laboratories, Kumamoto, Japan). This assay is based on the cleavage of 2-(2-methoxy-4-nitrophenyl)-3-(4-nitrophenyl)-5-(2,4-disulfophenyl)-2H-tetrazolium, monosodium salt (WST-8) to formazan dye by the mitochondrial dehydrogenase enzyme. After incubation with WST-8 for 2 hours at 37°C, the absorbance was measured at 450 nm using a microplate leader. The absorbance was directly proportional to the number of living cells (data not shown).

Animals

Adult RCS rats and age-matched Wistar rats were maintained humanely with proper institutional approval, and in accordance with the statement of the Association for Research in Vision and Ophthalmology. All animal experiments were performed under approved protocols and in accordance with the recommendations for the proper care and use of laboratory animals by the Committee for Animals, Recombinant DNA, and Infectious Pathogens Experiments at Kyushu University and according to The Law (no.105) and Notification (no.6) of the Japanese Government.

Gene Transfer Procedures

The subretinal injection of each solution was performed as previously described.[11,25] Briefly, 3-week-old RCS rats were anesthetized by inhalation ether. A 30-gauge needle was inserted into the subretinal space of the peripheral retina in the nasal hemisphere via an external

transscleral transchoroidal approach. The vector solution (SIV-hPEDF or SIV-Empty; 2.5×10^7 transducing U/ml × 10 μl) was injected, and excess solution from the injection site was washed out using PBS. Approximately 3 μl of solution remained in the subretinal space (data not shown). The appearance of a dome-shaped retinal detachment confirmed the subretinal delivery. Eyes that sustained prominent surgical trauma, such as retinal or subretinal hemorrhage or bacterial infection, were excluded from this examination.

Histological Examination

At 2 weeks after gene transfer, the eyes of animals were enucleated and frozen in liquid nitrogen, and 5-μm-thick cryosections were prepared along the horizontal meridian. The sections were stained with hematoxylin and eosin, and the number of photoreceptors was counted per 100 μm at 10 points as previously described (A1 to A5: from the ora serrata to the optic nerve of the nasal hemisphere; A6 to A10: from the optic nerve to the ora serrata of the temporal hemisphere).[11]

Immunocytochemistry

R28 cells were fixed in 4% paraformaldehyde for 15 minutes, and then rinsed with PBS at room temperature. The cells were blocked with 3% nonfat dried milk and labeled with rabbit anti-AIF antibody (1:100; Cell Signaling Technology, Danvers, MA) at 4°C for 24 hours. After biotinylated goat anti-rabbit IgG (H+L) (1:200; Vector Laboratories, Burlingame, CA) was used as a secondary antibody, the cells were incubated with r-phycoerythrin (PE)-conjugated or fluorescein isothiocyanate-conjugated streptavidin (1:100; BD Biosciences, San Diego, CA). After labeling, propidium iodide or 4,6-diamidino-2-phenylindole (DAPI) was used to counterstain the nuclei. Immunofluorescence images were acquired using an Olympus BX51 microscope with a fluorescent attachment (Tokyo, Japan). For negative controls, the primary antibody was omitted.

Immunohistochemistry

Rats were sacrificed under deep anesthesia. The eyes were removed and frozen in OCT compound (Sakura Finetechnical Co., Tokyo, Japan). Five-μm-thick sections were cut, air-dried, and fixed in cold acetone for 10 minutes. For a primary antibody, rabbit anti-AIF antibody (1:100; Cell Signaling Technology) was used. The specimens were imaged with a laser-scanning confocal microscope (LSM-GB200, Olympus).

Terminal dUTP Nick-End Labeling (TUNEL) Staining

The TUNEL procedure and quantification of TUNEL-positive cells were performed using an ApopTag fluorescein direct *in situ* apoptosis detection kit (Chemicon International, Temecula, CA) for R28 cultures or an Apoptosis Detection TACS TdT Kit (R&D Systems) for retinal sections according to the instructions of the manufacturer. The number of TUNEL-positive cells was counted in a masked manner.

Flow Cytometry Analysis

The population of early apoptotic cells was analyzed using an Annexin V-PE Apoptosis Detection Kit I (BD Biosciences). After serum starvation, R28 cells were harvested, washed twice with ice-cold PBS, and resuspended in 100 μl of calcium-binding buffer (10 mmol/L Hepes/NaOH, pH 7.4, 140 mmol/L NaCl, 2.5 mmol/L $CaCl_2$). The cells were double-labeled with Annexin V-PE (1:20) for the assessment of phosphatidylserine exposure and 7-amino-actinomycin D (7-AAD) (1:20) for cell viability analysis. After 15 minutes of incubation in the dark, the cells were diluted with 400 μl of binding buffer. Samples were analyzed in a FACScan flow cytometer (Becton Dickinson, San Jose, CA) using the program CellQuest (Becton Dickinson) for subsequent data treatment. A total of 5000 events per sample were acquired, and Annexin V-PE-positive and 7-AAD-negative events were defined as early apoptotic cells.

Western Blotting

Eighty μg of protein was separated on sodium dodecyl sulfate-polyacrylamide gel electrophoresis and transferred to the membrane. After blocking with 3% nonfat dried milk, the membrane was reacted with anti-AIF antibody (Calbiochem, San Diego, CA), anti-cleaved caspase-3, anti-Bcl-2, or anti-Bax antibody (Cell Signaling Technology). The immunoreactivity was visualized using the ECL Plus detection reagents (Amersham Biosciences, Buckinghamshire, UK).

Enzyme-Linked Immunosorbent Assay (ELISA)

The protein contents in rat eyes were determined using an ELISA kit for human PEDF (not available for rat PEDF; Chemicon International). For ocular tissue preparation, conjunctival and muscular tissues were removed from enucleated eyes. The eyes were washed with PBS, minced with scissors in 500 μl of 1× lysis buffer with a protease inhibitor cocktail, and centrifuged at 15,000 rpm for 5 minutes at 4°C. The supernatants were subjected to ELISA according to the manufacturer's instructions.

RNAi

AIF siRNA was synthesized with the sequence 5′-GCAACCUAGUAUACUUCUUTT-3′. The scrambled counterpart, control siRNA, had the sequence 5′-GCAUCGAAUAUUCUAC-CUUTT-3′. The sequence of Bcl-2 siRNA was 5′-AUGGAUGUACUUCAUCACGAUCUCC-3′, and the negative control kit Medium GC was used as a control (Invitrogen). Transfection of 40 nmol/L siRNA was performed using Lipofectamine 2000 reagent (Invitrogen) according to the manufacturer's instructions.

RNA Extraction and Quantitative Real-Time Polymerase Chain Reaction (PCR)

The procedures for RNA extraction were described previously.[26] The total RNA was extracted from the R28 cells or the neural retina by Isogen (Nippon Gene Co., Osaka, Japan) followed by treatment with RNase-free DNase I. The RNA was then reverse-transcribed and amplified with the TaqMan EZ RT-PCR kit and a sequence detection system, model 7000 (Applied Biosystems, Foster City, CA). The PCR primers used in this study were as follows: rat Bcl-2 forward, 5′-CTGGGATGCCTTTGTGGAA-3′, rat Bcl-2 reverse, 5′-CAGAGACAGCCAGGAGAAATCA-3′; rat Bcl-2 hybridization probe, 5′-FAM-ATGGCCCCAGCATGCGACCTC-TAMRA-3′; rat Bax forward, 5′-CGTGGTTGCCCTCT TCTACTTT-3′, rat Bax reverse, 5′-TGATCAGCTCGGGCACTTTA-3′; rat Bax hybridization probe, 5′-FAM-CTAGCAAACTGGTGCTCAAGGCCCTG-TAMRA-3′; rat β-actin forward, 5′-CCCTGGCTCCTAGCACCAT-3′; rat β-actin reverse, 5′-CCTGCTTGC-TGATCCACATCT-3′; and rat β-actin hybridization probe, 5′-FAM-CCTGGCCTCACTGTCCACCTTCCA-TAMRA-3′. The expression level of the target gene was normalized by the β-actin level in each sample.

MitoTracker Staining

R28 cells were incubated with a 50 nmol/L solution of MitoTracker Orange CMTMRos (Invitrogen), a derivative of tetramethylrosamine, for 15 minutes at 37°C. The MitoTracker probe passively diffuses across the plasma membrane and accumulates in active mitochondria, driven by the mitochondrial inner transmembrane potential.[27,28] After incubation, the cells were fixed in 4% paraformaldehyde for 15 minutes, labeled with DAPI, and observed under a fluorescence microscope.

Statistical Analyses

All values were expressed as the mean ± SD. The data were analyzed by the two-tailed unpaired Student's *t*-test. Numbers per group were as indicated. A *P* value less than 0.05 was considered statistically significant.

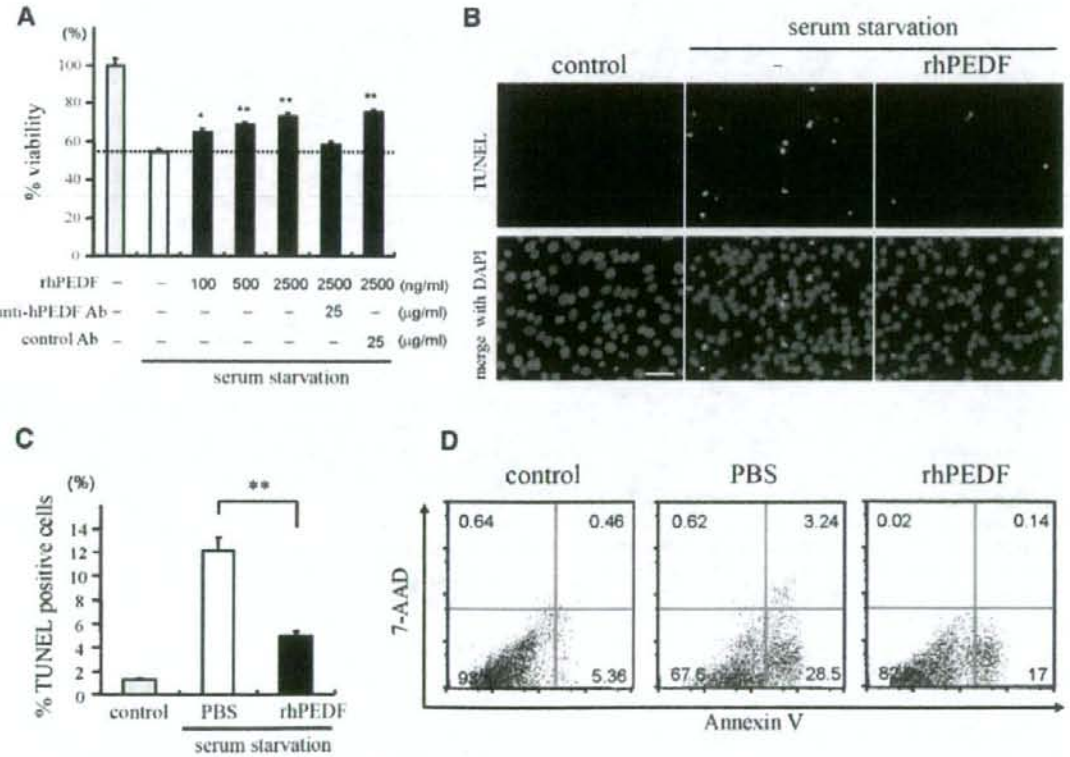

Figure 1. PEDF rescues apoptosis induced by serum starvation in R28 cells. **A:** The effect of PEDF on cell viability. R28 cells were serum-deprived and treated with PBS or rhPEDF at the indicated doses. After 48 hours of culturing, the cell viability was assessed by WST-8 colorimetric assay ($n = 4$ each). The effect of PEDF was reversed by anti-PEDF antibody but not by nonimmune control antibody. $^{*}P < 0.05$ and $^{**}P < 0.01$ versus PBS-treated samples. **B** and **C:** TUNEL staining (**B**) and quantitative analysis of the TUNEL-positive apoptotic nuclei (**C**) in serum-starved R28 cells treated with PBS (white bar) or rhPEDF (black bar) ($n = 5$ each). The cells growing in serum-containing medium were used as controls (gray bar). $^{**}P < 0.01$. **D:** Flow cytometry analysis of the apoptotic population after 48 hours of serum starvation. Cells were stained with Annexin V and 7-AAD. The percentages of Annexin V-positive and 7-AAD-negative early apoptotic cells were 28.3 ± 0.15% in PBS-treated cells and 17.7 ± 0.34% in rhPEDF-treated cells ($n = 4$ each). Scale bar = 50 μm.

Results

Effects of PEDF on Serum Starvation-Induced Apoptosis in R28 Cultures

The R28 cell line was derived from the rat retina on postnatal day 6 and has been shown to express neuronal genes.[29] To investigate whether PEDF can act as a survival factor for R28, we first cultured R28 cells under a serum-starved condition with or without rhPEDF, and assessed the cell viability by WST-8 colorimetric assay after 48 hours of culturing. Treatment with rhPEDF dose dependently rescued serum starvation-induced cell death and 41.1% of the reduction of cell viability was rescued by 2500 ng/ml rhPEDF ($P < 0.01$ versus PBS-treated R28 cells; Figure 1A). The effect of rhPEDF was completely reversed by treatment with polyclonal anti-hPEDF antibodies (25 μg/ml) (Figure 1A). The vitreous of the human eye contains 0.5 to 5 μg/ml of hPEDF protein,[30,31] and thus the concentrations of rhPEDF used in this experiment were in a physiological range. TUNEL staining revealed that ~10% of cells were TUNEL-positive apoptotic cells after 48 hours of serum starvation (12.2 ± 1.13%); by contrast, treatment with rhPEDF significantly reduced the frequency of TUNEL-positive cells (5.1 ± 0.26%, $P = 0.0002$; Figure 1, B and C). Less than 2% of cells were TUNEL-positive under control conditions. The apoptotic population was also assessed by fluorescence-activated cell sorter analysis of Annexin V/7-AAD staining. The percentages of early apoptotic cells that were defined as Annexin V-PE-positive and 7-AAD-negative were significantly lower in rhPEDF-treated cells (17.7 ± 0.34%) than PBS-treated cells (28.3 ± 0.15%, $P < 0.0001$; Figure 1D). Together, these results indicate that PEDF inhibits the apoptosis induced by serum starvation in R28 cells. RT-PCR analysis revealed that R28 cells strongly expressed the PEDF receptor, which was identified in a recent study (data not shown).[32]

A Minor Role of Caspases in Serum Starvation-Induced Apoptosis in R28 Cells

To elucidate the molecular events during serum starvation-induced apoptosis, we next examined the involvement of caspases. First, we performed Western blot analysis of caspase-3, a key effector of caspase-dependent apoptosis. As shown in Figure 2A, a 17-kDa active form of caspase-3 was detected at 48 hours after serum starvation. To elucidate the exact contribution of caspases, we next cultured R28 cells under a serum-starved condition, in the presence or absence of Z-VAD-fmk, a broad range caspase inhibitor. Treatment with Z-VAD-fmk (10 μmol/L) completely abrogated the cleavage of caspase-3 induced by serum starvation (Figure 2A), but this treatment showed no beneficial effect on the cell viability (Figure 2B). The doses higher than 10 μmol/L were cytotoxic, reducing the levels of cell viability (data not shown). These results suggest that caspases are not the major executioners of serum starvation-induced apoptosis. By contrast, the cell death induced by staurosporine, a potent activator of caspases, was significantly rescued by treatment with Z-VAD-fmk (10 μmol/L) (Figure 2C). Interestingly, rhPEDF had no significant effect on either the cell viability or the cleavage of caspase-3 after staurosporine treatment (Figure 2, C and D), suggesting that PEDF might be involved in a caspase-independent pathway.

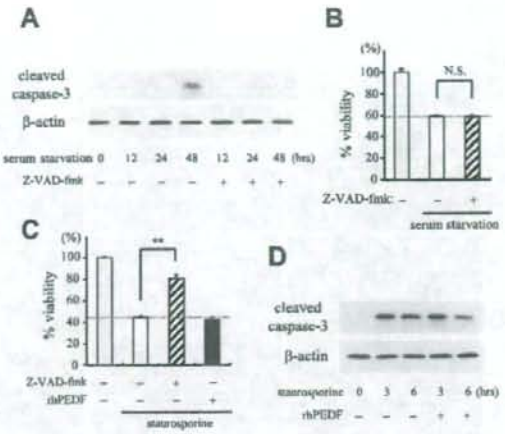

Figure 2. The role of caspases in serum starvation-induced apoptosis. **A:** Analysis of activation of caspase-3 after serum starvation. Total proteins were purified from R28 cells that were serum-deprived for the indicated period of time with or without Z-VAD-fmk (10 μmol/L), and subjected to Western blotting with an antibody against cleaved caspase-3 (**top**). Lane-loading differences were normalized by the level of β-actin (**bottom**). The panels show the representative results from three independent experiments. **B:** The inhibition of caspases did not rescue serum starvation-induced cell death. R28 cells were cultured under a serum-starved condition for 48 hours in the presence or absence of Z-VAD-fmk (10 μmol/L) before assessing the cell viability ($n = 4$ each). **C:** Staurosporine-induced cell death was rescued by Z-VAD-fmk, but not by PEDF. R28 cells were cultured with 100 nmol/L staurosporine for 24 hours in the presence of PBS, Z-VAD-fmk (10 μmol/L), or rhPEDF (2500 ng/ml), and the cell viability was assessed ($n = 4$ each). $^{**}P < 0.01$. **D:** The effect of PEDF on caspase-3 activation induced by staurosporine. Total proteins were purified from R28 cells that were treated with staurosporine for the indicated period of time with or without rhPEDF (2500 ng/ml). Western blotting showed that the expression level of cleaved caspase-3 was unchanged by rhPEDF.

Role of AIF in Serum Starvation-Induced Apoptosis and Effects of PEDF on AIF Relocalization

AIF is a mitochondrial flavoprotein that is released in response to death stimuli and induces apoptosis independently of caspases after nuclear translocation.[20] To examine whether serum starvation-induced apoptosis involved AIF, we next analyzed the changes in subcellular localization of AIF by immunocytochemistry. In control R28 cells, AIF was excluded from the nucleus and displayed a punctate staining pattern in the cytoplasm. By contrast, after 48 hours of serum starvation, 17.5 ± 4.6% of the cells showed diffuse staining and nuclear translocation of AIF (Figure 3, A and B). No positive staining was found by nonimmune IgG (data not shown). Double-labeling with TUNEL showed that ~75% of AIF-positive nuclei were also TUNEL-positive (Figure 3, C and D). Furthermore, treatment with rhPEDF dramatically pre-

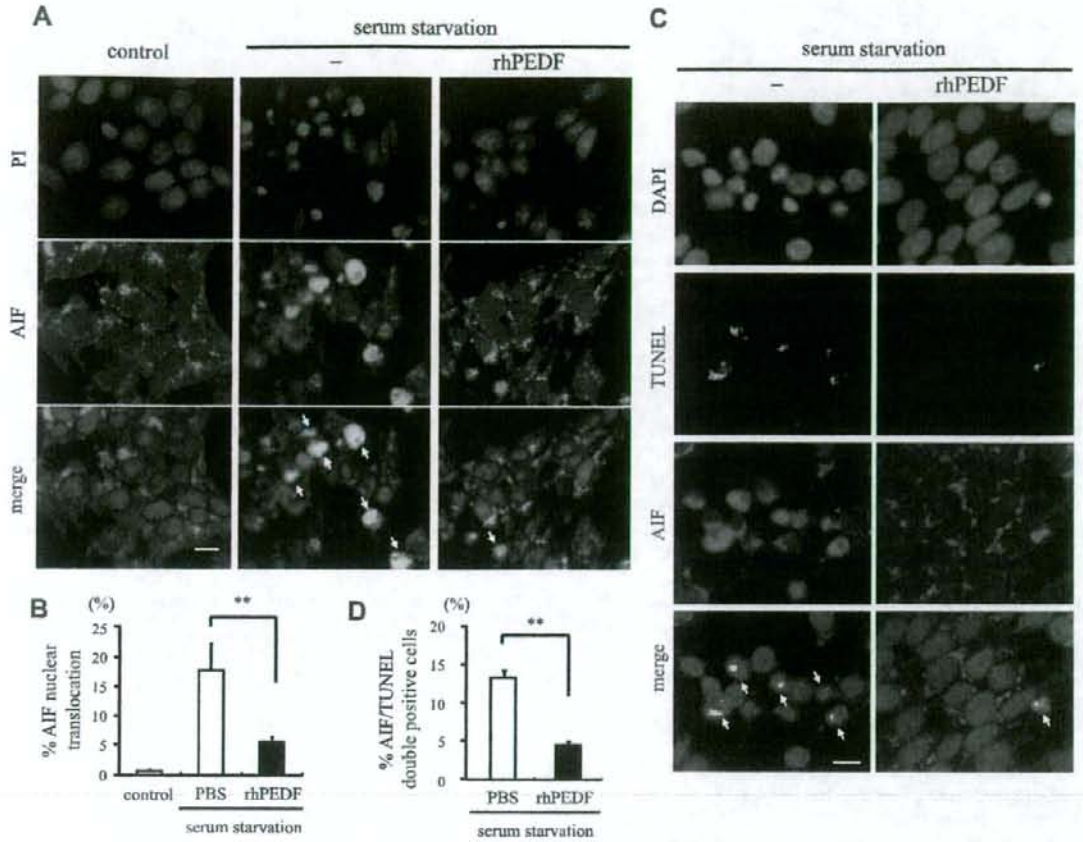

Figure 3. AIF nuclear translocation during serum starvation-induced apoptosis and effect of PEDF on the AIF release. **A:** Immunocytochemistry of AIF after serum starvation. After 48 hours of culturing in serum-starved medium with or without rhPEDF (2500 ng/ml), the R28 cells were stained with an anti-AIF antibody. The cells growing in serum-containing medium were used as controls. The nuclei were counterstained with propidium iodide. **Arrows** indicate the translocation of AIF into the nucleus. **B:** Quantification of cells showing nuclear translocation of AIF in control (gray bar) or serum-starved R28 cells treated with PBS (white bar) or rhPEDF (black bar) ($n = 5$ each). $^{**}P < 0.01$. **C** and **D:** Double-staining for AIF and TUNEL (**C**) and the quantification of AIF/TUNEL double-positive apoptotic nuclei (**D**) after serum starvation ($n = 5$ each). The nuclei were counterstained with DAPI. **Arrows** indicate the co-localization of AIF and TUNEL. $^{**}P < 0.01$. Scale bars = 10 μm.

vented the nuclear translocation of AIF after serum starvation (5.6 ± 0.74%, $P = 0.0066$ versus PBS-treated samples; Figure 3, A and B) and reduced the number of AIF/TUNEL double-positive cells ($P < 0.0001$ versus PBS-treated samples; Figure 3, C and D).

To further address the role of AIF in serum starvation-induced apoptosis, we used RNAi to knockdown AIF in R28 cells. siRNA for AIF, but not randomized control siRNA, showed efficient down-regulation of AIF (Figure 4A). When AIF was down-regulated, 33.1% of the reduction of cell viability after 48 hours of serum starvation was rescued ($P = 0.0002$ versus R28 cells treated with randomized control siRNA; Figure 4B). TUNEL-positive apoptotic cells were also significantly reduced in cells treated with siRNA for AIF (6.6 ± 1.30%) compared to cells treated with randomized control siRNA (13.6 ± 0.76%, $P = 0.0031$; Figure 4, C and D). In addition, treatment with rhPEDF showed no significant effect on the frequency of TUNEL-positive cells in samples with AIF down-regulation (5.39 ± 1.11%, $P = 0.53$; Figure 4, C and D). Together, these results indicate that AIF is an important executioner of serum starvation-induced apoptosis, and that PEDF inhibits the apoptosis by preventing the AIF nuclear translocation.

PEDF Prevents AIF Translocation and Photoreceptor Apoptosis in RCS Rats

To further examine the role of PEDF *in vivo*, we next assessed the effect of exogenously overexpressed PEDF on the degeneration of photoreceptors in RCS rats. P21 RCS rats received subretinal injection of SIV-hPEDF or SIV-Empty in the nasal peripheral retinas. First, we confirmed the efficient gene transfer and expression of hPEDF after subretinal injection of SIV-hPEDF by ELISA (Figure 5A). The gene transfer of hPEDF was observed in the RPE in the vector-injected area as previously de-